SPECIFIC HEAT OF UPd_2Si_2

By

Tatiana Startseva

B. Sc. (Physics) Belarus State University

A THESIS SUBMITTED IN PARTIAL FULFILLMENT OF

THE REQUIREMENTS FOR THE DEGREE OF

MASTER OF SCIENCE

in

THE FACULTY OF MATHEMATICS AND SCIENCE

DEPARTMENT OF PHYSICS

We accept this thesis as conforming

to the required standard

.....

.....

.....

.....

.....

BROCK UNIVERSITY

August 1994

In presenting this thesis in partial fulfilment of the requirements for an advanced degree at Brock University, I agree that the Library shall make it freely available for reference and study. I further agree that permission for extensive copying of this thesis for scholarly purposes may be granted by the head of my department or by his or her representatives. It is understood that copying or publication of this thesis for financial gain shall not be allowed without my written permission.

Department of Physics
Brock University
500 Glenridge Avenue
St. Catharines, Ontario
Canada L2S 3A1

Date:

Abstract

The specific heat of single-crystal UPd_2Si_2 has been studied using both the step heating and continious heating methods for the temperature range 2 to 250 K. Successive phase transitions at $T_1 = 136K$ and $T_2 = 108K$ are reported, which are consistent with current publications. The transition at 40K, which was previously reported, has not been detected. Recent published elastic neutron scattering data , magnetic susceptibility and resistivity results suggest that UPd_2Si_2 may be a heavy fermion compound, however, the electronic specific heat coefficient γ $(= 18.97\frac{mJ}{gK^2})$, obtained from the specific heat C_v measurements, is smaller than that of the conventional heavy fermion system. The Debye temperature of UPd_2Si_2 is found to be 116.55K. The possibility is discussed that the maximum in C/T in the low-temperature range 2 to 4K corresponds to Schottky anomaly induced by localized magnetic impurities.

Table of Contents

Abstract ii

Acknowledgement viii

1 Introduction 1

2 Heavy–Fermion Materials 3

3 Specific heat. Theory of Heat Capacity and Calorimetric Methods 8

3.1 Calorimetric methods 8

3.1.1 Step heating method 8

3.1.2 Continuous heating method (Sweep method) 11

3.2 Theory of the heat capacity 13

3.2.1 Electronic and lattice specific heat at low temperature 13

3.2.2 Magnetic Contribution to the Specific Heat 15

3.2.3 Schottky effect 17

3.3 Principles of data processing 19

3.3.1 Sources of errors 20

3.3.2 Measurement of heating and cooling gradients 20

3.3.3 Correction of the temperature rise during heating 22

3.3.4 Temperature variation of specific heat 23

4 Calorimeter Design 27

5 Specific Heat of UPd_2Si_2 **37**

5.1 UPd_2Si_2 37

5.2 Experiment 43

5.2.1 Specific heat data at high temperature (Step method) 43

5.2.2 Specific heat data using Sweep method 44

5.2.3 Specific heat data at low temperature 48

6 Conclusions **56**

Appendices **57**

A Listing of RC-filtering program **57**

Bibliography **65**

List of Tables

2.1 Comparison of heavy fermion systems and normal metals 6

5.1 Parameters β, γ and Debye temperature calculated using different fits . 54

5.2 Electronic specific heat coefficient γ for various compounds 55

List of Figures

3.1 Schematic diagram of a set-up for measuring the heat capacity 9

3.2 The principle of the step heating method 10

3.3 The principle of the continuous heating method 12

3.4 The experimental data of a complete measuring cycle for an automated, adiabatic calorimeter 21

3.5 The extrapolation process when temperature is dropping during data collection 24

3.6 Comparison of data obtained using different temperature increments . . 26

4.1 The Sample holder 28

4.2 Calibration of the Germanium resistor 30

4.3 The Cryostat 32

4.4 The specific heat of Copper (temperature range 30–50K) 34

4.5 The specific heat of Copper (temperature range 140–220K) 36

5.1 Crystal structure of UPd_2Si_2 38

5.2 Magnetic structure of U-sublattice in the three phases 39

5.3 Specific heat of the UPd_2Si_2 single crystal as a function of temperature (temperature range $75K$ – $250K$) 41

5.4 Specific heat of the UPd_2Si_2 single crystal as a function of temperature (temperature range $30K - 70K$) 42

5.5 Specific heat of UPd_2Si_2 from measurements using the Sweep method. Phase transition at 104K 45

5.6 Specific heat of UPd_2Si_2 from measurements using the Sweep method. Phase transition at 136K 46

5.7 Specific heat of the UPd_2Si_2 single crystal as a function of temperature (temperature range 2K – 10K) 49

5.8 Specific heat of the UPd_2Si_2. Attempt to fit the data to spin-fluctuation term 50

5.9 Specific heat of UPd_2Si_2. The "Schottky-like" anomaly is subtracted away 51

5.10 Three contribution to the low-temperature specific heat of UPd_2Si_2 . . 52

5.11 Temperature dependence of the different contributions to the specific heat of UPd_2Si_2 53

Acknowledgement

I would like to take this opportunity to thank my supervisor, Dr. F.S. Razavi, with whom I have had the pleasure to work for the past two years, for his invaluable insights, guidance, enthusiasm and patience. He spent a tremendous amount of time advising, reassuring and supporting me.

I wish to thank Dr. B.Mitrović who encouraged my interest and spent his time in discussions. I offer sincere thanks to Dr. E.Sternin for his useful advice and for providing me with many unique opportunities throughout my graduate studies (especially, in area of computers).

A warm 'thank you' goes out to all the members of the Physics Department for their support and help. As well, thanks to the glassblower, John Vandenhoff and the guys from the machine and electronic shops for their excellent, speedy work which kept the lab running smoothly.

Thanks should also be given to Jim Murdoch for his huge contribution in my ability to speak English more or less properly and for his constant 'moral support'. I also would like to say thanks to Andrej Dobos for helping me with the RC-filter program.

Finally, to my grandparents, Tamara and Alex Lushpihan, whose encouragement and love helped me to persist in my studies, for their faith in me and for their constant support, which made this all possible, I express my love and my deepest gratitude.

Chapter 1

Introduction

The exploration of UT_2Si_2 (where T is Ru,Ni,Pd) [1, 2, 3] has generated intense interest and has led to numerous structural studies and measurements of the physical properties of these compounds. Interpretation of the measurements is in most cases complicated. Furthermore, the specific heat measurements, in particular, have been neither detailed nor extensive enough to establish the nature of the heat capacity behavior in the low–temperature range.

Heavy-fermion compounds (HFCs) possess a characteristically enormous low temperature electronic specific heat parameter γ. The material UPd_2Si_2, which has been the target of our research, can be considered as a potential heavy -fermion system (HFS). This assumption is based on elastic neutron scattering data [2], and on magnetic susceptibility and resistivity measurements [4]. To complete the picture of the properties of UPd_2Si_2 specific heat data was needed. Low temperature (1–4K) data, in particular, could be used to obtain the value of γ.

The measurements on conventional HFCs [1, 5, 6, 7] are more complete and better understood than those for compounds which have an electronic specific heat parameter γ smaller than that of a HFC [3] , but higher than that of the normal metals. This suggests that a comparison with HFCs is one way to interpret the specific heat of UPd_2Si_2. [5]. Such an approach is not entirely satisfactory, because the current understanding of the specific heat of HFC's is in itself incomplete. Nevertheless, this seems to be the most promising approach, and it is the one taken here.

Specific heat,$C - P$, is a characteristic property of the microscopic properties of a physical system. In general, different types of contributing excitations, e.g. phonons, spins, and lattice phase transitions are well-known [8]. The behavior of C_p gives information on the transitional energy (enthalpy ΔH_t; entropy ΔS_t) and, frequently, on the order of the transition : (1) for electronic (e.g. superconducting), magnetic, lattice structural (crystallographic) transitions, or for melting; and (2) for Schottky anomalies (two-level system), and order-disorder phenomena. The actual temperature where a transition from one phase to another occurs, can be detected by a specific heat experiment. The phase transitions are the other reason for our interest in the specific heat of UPd_2Si_2. Its measurement can complement recent elastic neutron scattering data by Shemirani *et al.* [2] and electrical resistivity measurement by Barati *et al.* [4] on this compound. These experimental data are in disagreement with the elastic neutron scattering data by Ptasiewicz-Bak *et al.* [9] over the number of phase transitions and the temperatures in which they occur . The specific heat results on a single crystal of UPd_2Si_2 reported herein will be compared to these data reported in the literature.

This thesis is organized into five sections: Section 2 is a brief summary of the information available on conventional heavy– fermion systems. Section 3 includes discussion of the experimental methods as well as the theory of specific heat. The construction of an experimental system built to measure the specific heat of small samples is described in Section 4. The data on the specific heat of UPd_2Si_2 is presented in Section 5.

Chapter 2

Heavy–Fermion Materials

Over the past years a new branch of metal physics has emerged [6, 5]. It deals with materials which are intermetallic compounds in which one of the constituents is taken from either the rare-earth or the actinide series, i.e. atoms with partially filled $4f$- or $5f$-electron shells. These so-called heavy fermion systems (HFS) include such materials as $CeCu_2Si_2$, UBe_{13}, UPt_3, URu_2Si_2, *etc.* At low temperature these materials behave as if these f electrons are localized at their atomic sites, as in conventional rare-earth and actinide compounds, where itinerant electrons are in states derived from loosely bound atomic s–, p– and d– orbitals. As these materials are cooled, the atomic moments due to partially – filled f-electron shells order spontaneously, usually in an antiferromagnetic configuration, less often in a ferromagnetic configuration. By contrast, in HFS some of the f–electrons become itinerant at low temperature and form a metallic state.

Ordinary metals can be visualized as a gas of electrons moving in a background of positively charged ions. This electron gas has the following low–temperature properties :

- specific heat varies linearly with temperature and the proportionality factor γ is the electronic specific heat parameter. γ for simple metals is of the order of 1 mJ/mole K.

- low–temperature magnetic susceptibility χ is independent of temperature. $\chi \sim 10^{-5}$ emu/mole.

In contrast, the properties of heavy fermion compounds are quite different. In HFS near room temperature ($\sim$ 300K), the rare earth or actinide elements that have magnetic moments associated with them form a sublattice. This sublattice has properties resembling those of weakly interacting magnetic moments immersed in a sea of conduction electrons with conventional masses. In other words, the sublattice has well–localized f-electrons [5] as well as ordinary conduction electrons with conventional masses. The susceptibility at room tempreature is Curie–type. At low temperature the system gains energy by losing magnetic moments. It happens because f-electrons are screened by s-, p- and d- electrons and become itinerant (not localized any more). A situation where due to an energy gain, a magnetic moment is lost, was first introduced in the Kondo effect. The latter concerns a single magnetic impurity embedded in a sea of conduction electrons. In the heavy-fermion system it seems that some of the features of the single Kondo impurity appear in a more pronounced form, because there is at least one magnetic ion per unit cell [10]. Therefore, heavy-fermion systems have sometimes been referred to as either "a lattice of Kondo ions" or "Kondo lattice systems".

At this point, it is instructive to discuss some low-temperature properties that are typical for heavy-fermion systems and distinguish them from ordinary metals. First, let us consider the electrical resistivity ρ. In ordinary metals ρ decreases rapidly with decreasing temperature below 300K from values that are of the order of 1 to $10\mu\Omega cm$. The temperature variation of the resistivity can be written as

$$\rho(T) = \rho_0 BT. \tag{2.1}$$

At room temperature heavy fermion materials show an anomalously large electrical resistivity ρ, typically greater than 100 $\mu\Omega cm$ [6], suggesting that the conduction electrons scatter from nearly every atom in the lattice (see Table 1.1). After passing through a maximum at a temperature below $\sim$100K [4], ρ decreases to a low value as $T \rightarrow 0K$. As

an intriguing fact, it was noted that ρ varies $\sim T^2$ at low temperatures :

$$\rho(T) = \rho_0 + AT^2. \tag{2.2}$$

The coefficient A in eq.2.2 is remarkably large, 30-40$\mu\Omega cm/K^2$, some six or seven orders of magnitude larger than the coefficient B of the linear term (see eq.2.1) of ordinary metals.

At high temperatures ($T \geq 100K$) the magnetic susceptibility exhibits the familiar Curie-Weiss behaviour [6], due to partially filled 5f-electron shells of individual atoms , i.e.

$$\chi \sim (T + \Theta_p)^{-1}, \tag{2.3}$$

where Θ_p is the paramagnetic Curie–Weiss temperature. One finds at high temperature this Curie-Weiss law with a negative intercept which goes over at low-temperature to a large constant value. As the heavy fermion state is reached, Pauli–like paramagnetism develops rather than magnetic ordering, presumably due to spin compensation's interactions.

Finally, a typical [6] temperature dependence for the specific heat C_P of the heavy electron materials is as follows. At high temperatures its behaviour is consistent with that of a usual metal. However, that is not the case at low temperatures. The electronic specific heat of the ordinary metals can be described fairly well by one single term

$$C_P^{el} = \gamma T \tag{2.4}$$

at temperatures below 10K. For ordinary metals a plot of C_P/T versus T^2 would be a straight line with a positive slope and an intercept of about 1mJ/mole K. For heavy fermion materials, in general, the ratio C_P/T rises considerably with decreasing temperature in the temperature range 1-4K and the values are greater than 100 mJ/mole K

[6]. The temperature dependence itself might be interpreted by stating that the parameter γ is no longer constant but is strongly temperature dependent. So far, no analytic expression for the temperature dependence of the specific heat in heavy fermions has been found. The only exception is, perhaps, UPt_3. Doniach and Engelberg [18] and Brinkman and Engelberg [19] predicted that in addition to the usual γT and βT^3 terms in the specific heat, spin fluctuation would produce a $\delta T^3 \ln T$ term. This expression has been used [5] in low temperature fits

$$\frac{C_P}{T} = \gamma_0 + \beta T^2 + \delta T^2 \ln T. \tag{2.5}$$

A very large value of the C_P^{el} (or γ) as T approaches 0K must be interpreted as evidence for an enormous density of states at the Fermi energy E_F. This implies very large effective masses for these electrons and hence provides the name now generally used for these systems.

For better comparison, the typical values of resistivity, susceptibility and electronic specific heat of ordinary metals and heavy fermion systems at low temperature are given in Table 2.1.

	Ordinary metals	HFS
1.	$\rho \sim 10 \mu\Omega cm$	$\rho \sim 200 \mu\Omega cm$
2.	$\chi \sim 10^{-5} emu/mole$	$\chi \sim 10^{-2} emu/mole$
3.	$\gamma \sim 1 mJ/moleK$	$\gamma \sim 100 mJ/moleK$

Table 2.1: Comparison of heavy fermion systems and normal metals

It is clear from the above that the heavy fermion compounds represent an exciting new class of materials. They do not fit into the traditional classifications of materials with partially filled atomic shells, namely metals, semiconductors or insulators. At high temperature, they are essentially indistinguishable from other rare - earth or actinide

intermetallic compounds with local moments arising from the partially filled f shells. But as temperature is lowered, instead of forming magnetically ordered structures as is usually the case, an itinerant or delocalized metallic state is formed. The theoretical understanding of how such a state arises out of the f electrons with their strong Coulomb interactions, is a very active problem at present and will, undoubtedly, lead to new insight into the many–body problem, in general.

Chapter 3

Specific heat. Theory of Heat Capacity and Calorimetric Methods

3.1 Calorimetric methods

3.1.1 Step heating method

The low-temperature calorimetry (LTC) and step–heating methods were proposed by W. Nernst in 1909. Today his adiabatic step-heating method is still the most precise type of calorimetric experiment for collecting the heat capacity data. Nernst's "pulse heating" method is a direct application of the definition of the specific heat

$$C_p(T) = \lim_{\Delta T \to 0}[\frac{Q}{\Delta T}], \tag{3.1}$$

where Q is the energy supplied to the sample holder [1] (including the heater which supplies a heat pulse to the sample and the thermometer which determines the sample temperature) assembly and ΔT is the temperature increment. Both Q and ΔT have to be determined as accurately as possible.

The sample and its holder are thermally insulated from the surroundings (adiabatic conditions). The schematic arrangement of the system is given in Figure 3.1 (after [11]). The principle of the step heating method is shown in Figure 3.2. Starting from a constant temperature T_A the sample assembly is heated by electrical power during a time Δt_H. If the power is turned off, an exponential decay of the temperature $T(t) = T_0 + \Delta T e^{-t/\tau_e}$ occurs with a time constant $\tau_e = C/K_e$ until the system reaches the new steady temperature T_E. The time constant τ_e ranges from 1-3 minutes. It is necessary to

[1] The sample holder or, more precisely, the sample chamber will be referred to further on as addenda.

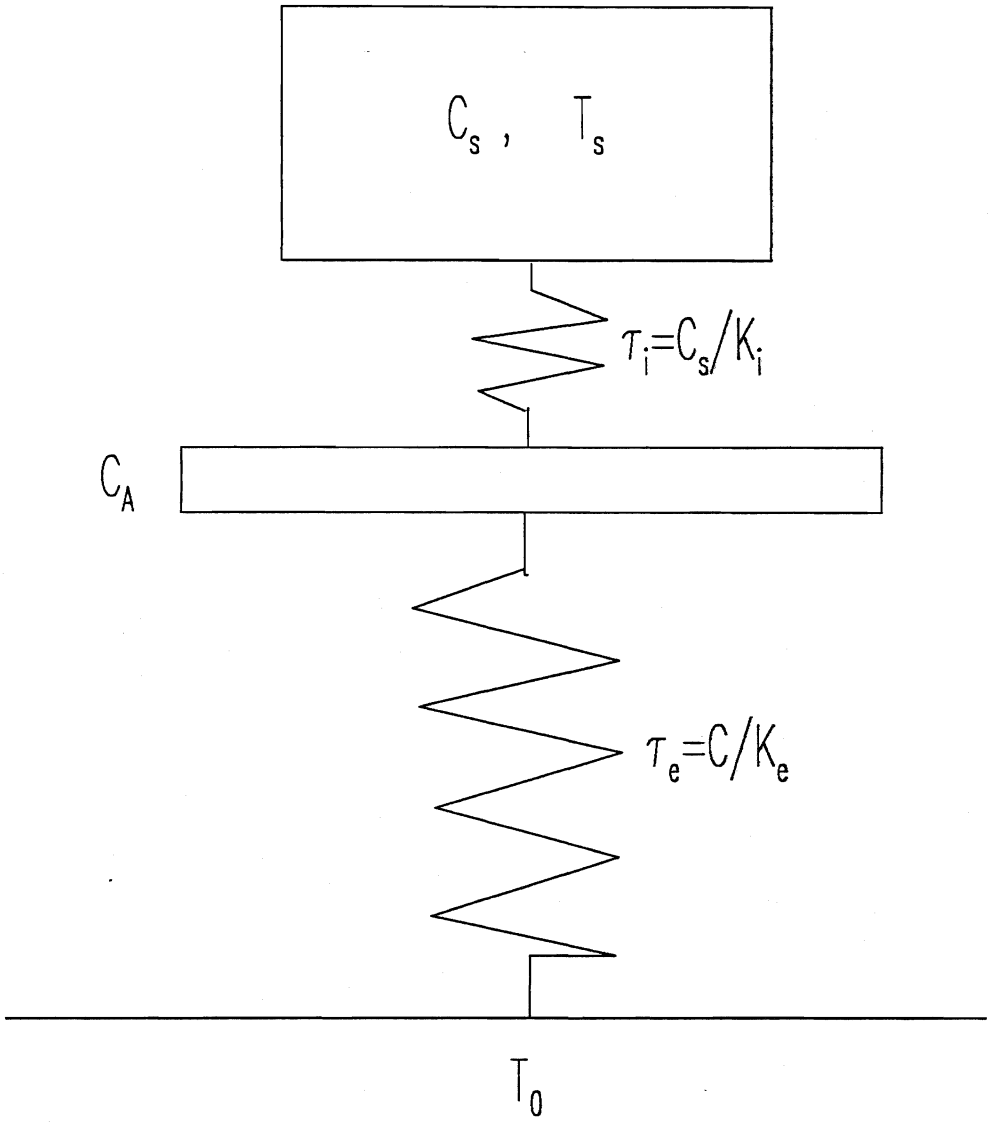

Figure 3.1: **Schematic diagram of a setup for measuring the heat capacity**
C_s and T_s are the heat capacity and the temperature of the sample. C_A is the heat capacity of the sample holder. T_0 is the temperature of the bath/surrounding. K_i and K_e are the internal and external thermal leaks (heat conductivities). τ_i, τ_e are the internal and external thermal relaxation times. For adiabatic calorimetry $\tau_i \ll \tau_e$, $\tau_e = \infty$ and for non–adiabatic calorimetry $\tau_i \gg \tau_e$, $0 < \tau_e < \infty$.

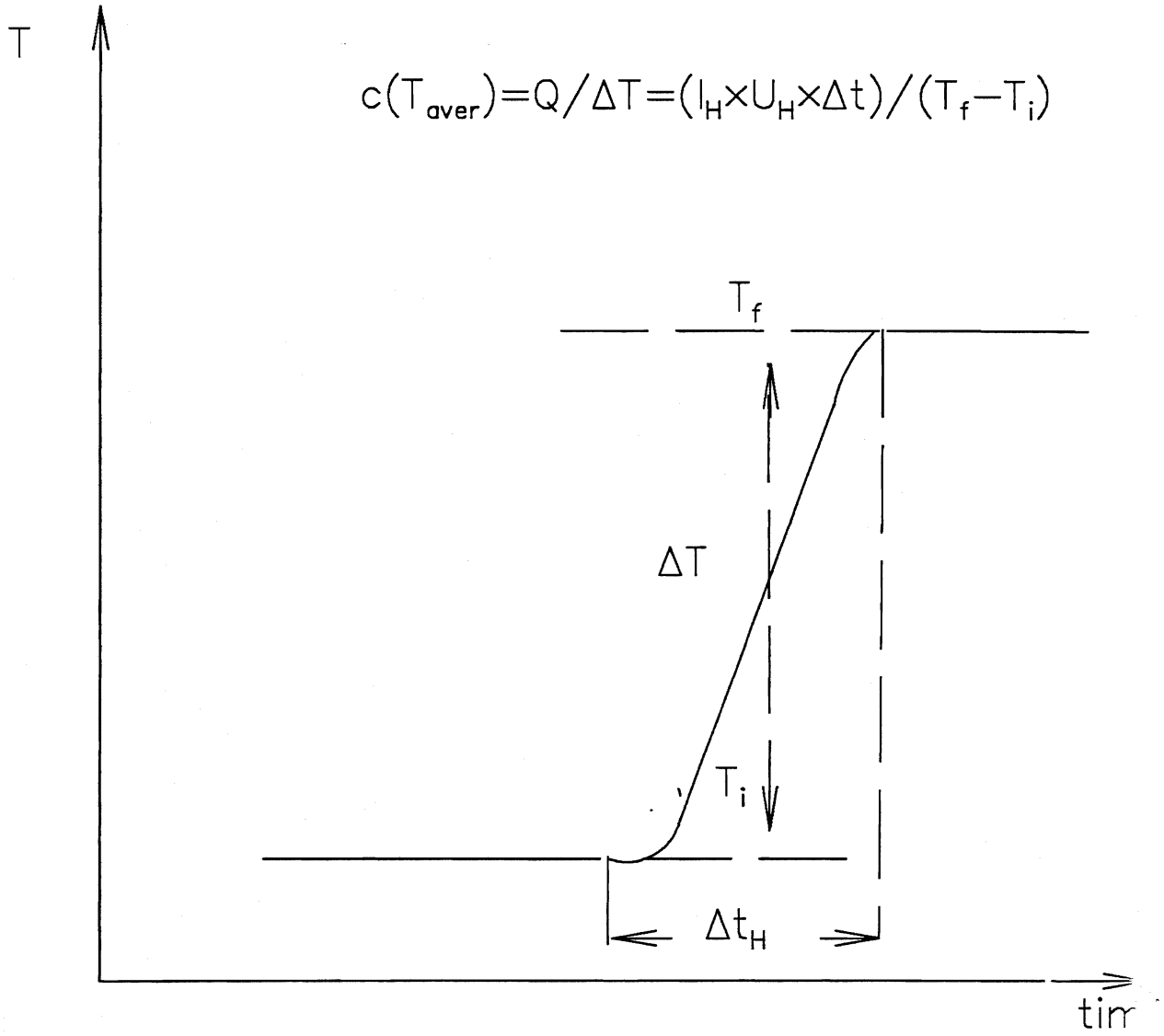

Figure 3.2: **The principle of the step heating method**
I_H is the heating current. U_H is the voltage across heater resistance. T_E is the final temperature (after heating). T_A is the initial temperature (before heating). Δt_H is the heating time. ΔT is the temperature increment.

wait for an equilibrium to be reached inside of the sample block which can be described by the external relaxation time (sample block) τ_e, provided that the internal relaxation time (inside of the sample) $\tau_i = C/K_i$ is short ($\tau_i \ll \tau_e$). Difficulties may arise if the internal relaxation time is slow. Fortunately, a temperature gradient within the sample has not been observed. The thermal equilibrium or steady-state temperatures are determined before and after electrical heat input Q by extrapolation to the initial and final temperature T_i and T_f, respectively, from which the temperature step $\Delta T = T_f - T_i$ is calculated. A small drift rate of the temperature is tolerable. The adiabatic conditions are ensured by placing one or two thermal shields around the sample, which work either under adiabatic conditions ($T_{sample} = T_{shield}$) or under isothermal conditions ($T_{sample} \geq or \leq T_{shield} = constant$). Calorimetry based on Nernst's method has remained a very tedious and time-consuming procedure. A run from 1.5 to 300K may require three weeks of measuring time. In addition, to achieve an accuracy of 0.1% rather large samples (10-100 g) are required.

3.1.2 Continuous heating method (Sweep method)

The continuous heating method was described by Junod [13]. The general principle of this method is shown in Figure 3.3 (reproduced from [12]). A constant power P is supplied to the sample. Let $\frac{dQ}{dt}$ be the heat exchange with the surrounding by conduction and radiation.

Then

$$P + \frac{dQ}{dt} = mC\frac{dT}{dt} \tag{3.2}$$

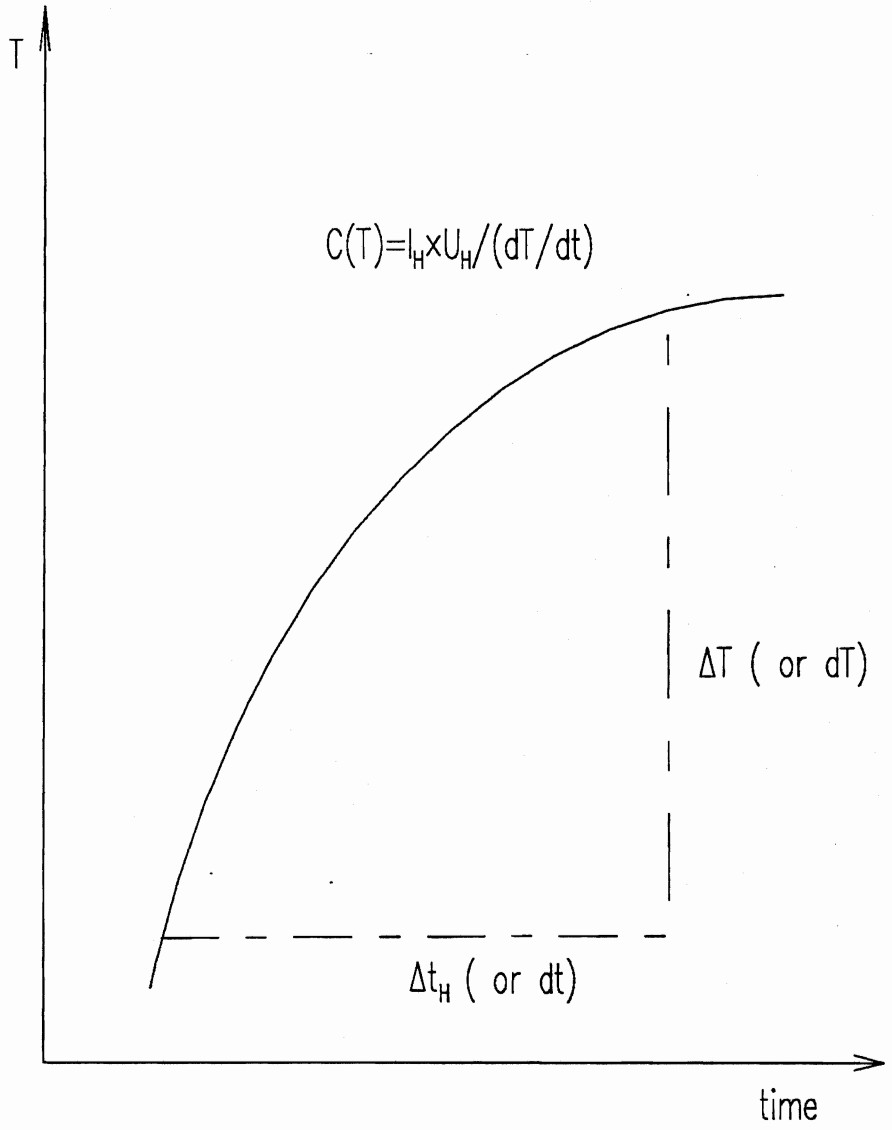

Figure 3.3: **The principle of the continuous heating methods**
I_H is the heating current. U_H is the voltage across heater resistance. Δt_H is the heating time and ΔT is the temperature increment. (in the formula above dT corresponds to ΔT on the graph and dt to Δt_H.

where m is the mass of the sample and C is the specific heat of the sample. If the heat power is turned off then,

$$\frac{dQ}{dt} = mC\frac{dT}{dt}. \tag{3.3}$$

Hence,

$$\frac{1}{C(T)} = \frac{m}{PI}\frac{dT}{dR}\left(\frac{dU(T)}{dT} - \frac{dU_0(T)}{dT}\right) \tag{3.4}$$

where I is the thermometer current, $\frac{dR}{dT}$ is the temperature coefficient of the platinum (germanium) resistor, $\frac{dU(T)}{dT}$ is a voltage drift, and $\frac{dU_0(T)}{dT}$ is a voltage drift across the thermometer. Over a narrow temperature range, $\frac{dR}{dT}$ can be considered, approximately, constant. $\frac{dU(T)}{dT}$ is then proportional to C^{-1} and the plot of $\frac{dU(T)}{dT}$ against U provides a representation of C^{-1} against T. Ideally, this technique requires an immediate distribution of heat within addenda. In reality, even if the net heat exchange with the surrounding is zero some time after the sample heater has been turned on, two temperature gradients will appear. The first gradient is across the layer of varnish which insulates the heater from the sample; the second is across the layer of the varnish that separates the sample thermometer from the heater. These gradients do not allow an immediate distribution of heat which leads to a small error in the specific heat data obtained by the continuous heating method. We have chosen this method because it is better suited for small samples of high thermal conductivity [11]. It has the additional advantages of speed and simplicity.

3.2 Theory of the heat capacity

3.2.1 Electronic and lattice specific heat at low temperature

The heat capacity has several components. The atoms in a solid vibrate about their mean position at the lattice sites, providing the lattice contribution to the specific heat.

The electronic contribution to C_P arises from the thermal excitation of free electrons (in metals). In some cases, the energy levels of bound electrons may be split into discrete levels. The transitions among the levels are known as excitation modes. This is yet another contribution to the specific heat. Contributions from all modes should be added together to form the total heat capacity.

While all these possible types of thermal excitations contribute to the heat capacity of the material, the specific heat depends also upon their variation with temperature. Some of the modes are excited over the entire temperature range and so contribute to the specific heat at all temperatures. The atoms in a lattice can vibrate at all temperatures and so the lattice contribution to the heat capacity C_l is significant at all temperatures. The free electrons in a metal have very high heat content, but their contribution is very small at room temperature compared with the lattice contribution. Although at room temperature the electronic contribution to the heat capacity C_e of a metal is insignificant compared to the lattice contribution, the situation is quite different at low temperatures. C_e decreases linearly with T, whereas C_l is proportional to T^3 at low temperatures. Therefore, at sufficiently low temperature, C_e is larger than C_l. Above about 4K, the lattice contribution dominates, while below that temperature the electronic part remains significant. In general, at liquid-helium temperature, both terms are of comparable magnitude and the observed specific heat is of the form

$$C = C_l + C_e = \beta T^3 + \gamma T. \tag{3.5}$$

A plot of C/T against T^2 should therefore be a straight line, (see Sec.5, Fig. 5.9). Such a plot allows one to determine both β and γ. From the equation

$$\beta = \frac{12\pi^4 R}{5}\Theta_D^3, \tag{3.6}$$

where $R = nk_B = 8.314(J/moleK)$, the Debye temperature Θ_D can be calculated.

3.2.2 Magnetic Contribution to the Specific Heat

The lattice and electronic contributions are present in the specific heat at all temperatures. In contrast, there are some modes which are excited over a restricted range of temperature.

As a simplification, we consider excitations in a system with two levels, kT_0 apart. At $T < T_0$ the thermal energy is insufficient to cause many excitations. At the other extreme, when $T > T_0$ the levels are equally populated and the net change in energy due to the excitations is, approximately, zero. Only at $T \sim T_0$ can transitions occur. As we scan the temperature, the absorption of energy takes place only in the vicinity of T_0. It appears as a sharp bump in the specific heat curve.

A similar picture can be seen in a system of atoms with magnetic moments. The magnetic moments of the atoms arrange themselves in different ways. At high temperature the moments have a random orientation (paramagnetism – disordered spins). The exchange interaction is able to overcome the thermal randomization of the spins at a sufficiently low temperature. For the material considered in this work, adjacent spins are aligned antiparallel at low temperature. The jump from one orientation of magnetic moments to another is associated with a phase transition that can be seen in the specific heat data. It is clear that, if the atoms of a substance possess permanent magnetic moments, the magnetic state depends very much upon the temperature, which means that interesting effects may be expected in the specific heat. The ideal ordered state (all spins at lattice sites are aligned at 0K along the Z axis) exists only in the absence of thermal agitation. At finite temperature, the spins at some sites may be excited to higher energy states, i.e. point in other directions. Such a distribution may be Fourier-analyzed into a set of waves, so–called spin waves [2]. It is interesting to compare the spin waves with

[2]Spin waves are oscillations in the relative orientations of spins on a lattice

the lattice waves [3]. At low frequencies, the normal modes of a lattice have a dispersion relation [8]

$$\omega \sim q$$

where the allowed modes in the spin system may be either

$$\omega \sim q^2$$

as in ferromagnets or

$$\omega \sim q$$

as in antiferromagnets.

The spin waves may be quantized into magnons, which play the same role in magnetic phenomena as phonons do in lattice dynamics. Magnons and phonons obey Bose–Einstein statistics. This fact allows calculation of the low-temperature specific heat of magnetic materials.

To summarize all of the contributions mentioned above, the total heat capacity may be expressed as

$$C = C_l + C_e + C_M + C_n, \tag{3.7}$$

where C_n is the nuclear contribution arising from the interaction of the nucleus with the effective magnetic field at the nucleus; C_M is the magnetic contribution arising from the electrons in unfilled $5f$ shells of the Uranium atoms; C_e is the usual electronic contribution; and C_l is the lattice contribution.

[3]Lattice waves are oscillations in the relative positions of atoms on a lattice

In antiferromagnetic metals, the conduction electrons give a specific heat proportional to T, the phonons give a T^3 – term and if the magnetic term is added , the low–temperature specific heat will be of the form

$$C = C_l + C_e + C_M = \beta T^3 + \gamma T + \delta T^3. \tag{3.8}$$

The temperature variation of the heat capacity will be dominated by the term with the lowest power of T, namely, the electronic term.

The temperature dependence of the spin wave specific heat in antiferromagnets is of the same form as the lattice contribution in the Debye T^3–region. This makes an experimental separation of the spin wave and lattice specific heats almost impossible. The magnetic contribution to the heat capacity near the critical temperature is expected to behave as

$$C_M = A\left|1 - \frac{T}{T_M}\right|^{-\alpha} \tag{3.9}$$

where α – is a small positive number. In the limiting case of $\alpha \to 0$ the alternate form

$$C_M = A \ln\left(1 - \frac{T}{T_M}\right) \tag{3.10}$$

may be more applicable. For further details the reader is referred to references [17, 8].

3.2.3 Schottky effect

In addition to the specific heat terms described above , there may be on extra contributions. This occurs when the lowest energy state of an atom is composed of two or more levels which are separated by a small energy $\frac{\epsilon_1}{k} = \Delta$. At temperatures very much below Δ, the atoms cannot be excited to the upper levels and they will all be in their lowest state. As temperature Δ is approached, some of the atoms will be excited to higher states. The jump requires energy and hence there will be an extra specific heat in this

region. At the temperatures much greater than Δ, all levels will be equally populated and so there will be no further excitation. Hence there will be no further contribution to the specific heat.

The atomic nucleus has a spin, and hence a magnetic moment. Due to interaction of the nuclear and the electron magnetic moments, there will be an extra splitting of the atomic levels. The splitting is a part of the hyperfine structure. The depopulation of the higher HFS levels will give rise to a Schottky specific heat anomaly.

Let there be n energy levels above the the ground state and let each level have a degeneracy g_i and energy ϵ_i, above the ground state energy. With N independent particles in the system , the mean energy at a temperature T is

$$E = \frac{N \sum_{i=0}^{i=n} \epsilon_i g_i e^{(-\epsilon_i/kT)}}{\sum_{i=0}^{i=n} g_i e^{(-\epsilon_i/kT)}} \tag{3.11}$$

The specific heat is obtained by calculating dE/dT. The simple case of two levels illustrates all of essential the features. For a two–level system,

$$E = \frac{N\epsilon_1 g_1 e^{(-\epsilon_1/kT)}}{g_0 + g_1 e^{(-\epsilon_1/kT)}}, \tag{3.12}$$

and the Schottky specific heat is

$$\begin{aligned} C_{Schottky} &= \frac{N\epsilon_1^2 g_0}{kT^2 g_1} \frac{e^{(-\epsilon_1/kT)}}{\left(1 + \frac{g_0}{g_1} e^{(-\epsilon_1/kT)}\right)^2} \\ &= R\left(\frac{\Delta}{T}\right)^2 \frac{g_0}{g_1} \frac{e^{(\Delta/T)}}{\left(1 + \frac{g_0}{g_1} e^{-\Delta/T}\right)^2}, \end{aligned} \tag{3.13}$$

where $\Delta = \epsilon_1/k$ is the energy separation measured in K. From the previous equation it is easy to see that

$$C_{Schottky} = R\left(\frac{\Delta}{T}\right)^2 \frac{g_0}{g_1} e^{(-\Delta/T)}, \qquad T \ll \Delta, \tag{3.14}$$

$$= Rg_0 g_1 (g_0 + g_1)^{-2} \left(\frac{\Delta}{T}\right)^2, \qquad T \gg \Delta. \tag{3.15}$$

Thus, at very low temperature, the Schottky specific heat rises exponentially in accordance with eq.3.14, passes through a maximum and at higher temperatures decreases with a T^{-2} dependence eq. 3.15.

3.3 Principles of data processing

Figure 3.4 demonstrates the complete measuring cycle during a heat step with the Step Heating Method. Each heating period is between two drift periods, where no heat is supplied to the sample. First the drift of the sample temperature, T, approximately, under isothermal shield conditions, is determined by several successive measurements at constant time intervals. At present, the drift curve may be determined from 20 - 30 temperature readings; the interval time can be selected between 2 and 100 sec [11]. We have chosen 20 sec. Then, the sample temperature is raised with a heating current during the time interval t_h. Both values of the current and of the time interval are precalculated by the computer in such a manner that a chosen relative temperature increase is achieved. Next, the sample is allowed to thermally equilibrate for a selected time t_r , adequately adapted to the internal thermal relaxation of the sample. Thereafter, the temperature drift is measured as before. The increase in sample temperature $\Delta T = T_f - T_i$ is obtained by a linear fit and extrapolation of the corresponding drift rates towards the midpoint of the heating time interval t_h. The calculated energy supplied to the sample during heating and the corresponding temperature rise yield the specific heat. The heat capacity at the average temperature T_M ,

$$C_P(T_M) = \frac{I_h V_h t_h}{T_f - T_i} \tag{3.16}$$

where

$$T_M = \frac{T_f + T_i}{2} \tag{3.17}$$

is calculated and the result is stored and printed on the computer monitor. Note that the temperature still rises after the heater is turned off and only after a certain time, the so–called relaxation time t_r, does the temperature of the system reach, approximately, a constant level, Drift 2 (see Figure 3.4). This rise of the temperature can be explained by a self–heating of the sample thermometer.
This procedure is executed entirely by computer.

3.3.1 Sources of errors

In principle the specific heat measurement is very simple as far as the physics is concerned. But in practice there are many complicating factors. Heat losses (or heat gains) are the most prevalent. The three sources of potential heat loss are conduction through the support wire and electrical leads, convection and conduction through the surrounding gas, and radiation. With the design of apparatus used, the first two are negligible compared with the effect of radiation, which was unavoidable.

The main complication of the measurement process, therefore, is the correction for the heat losses [24].

3.3.2 Measurement of heating and cooling gradients

If the rate of heat loss of the specimen with the heater off is L (where L is treated as positive when there is a heat loss to the surroundings), then the rate of cooling of the

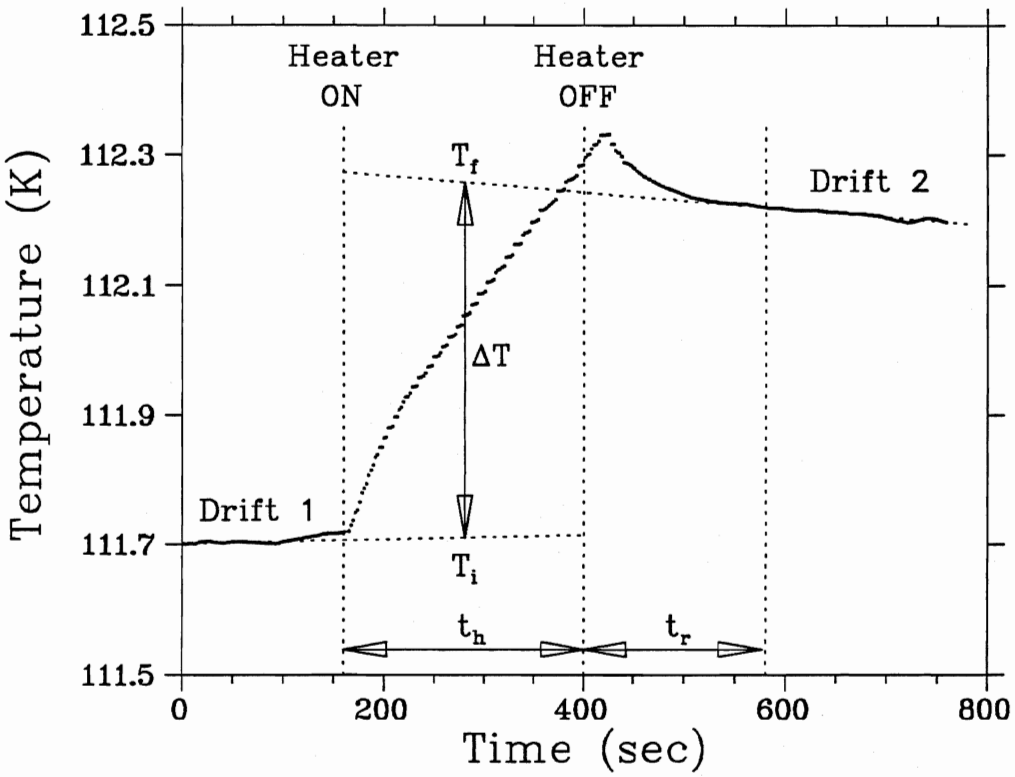

Figure 3.4: **The experimental data of a complete measuring cycle for an automated, adiabatic calorimeter**
ΔT is the temperature difference between the temperature before heating T_i and after T_f. t_h is the heating time. t_r is the relaxation time.

specimen will be

$$\left(\frac{dT}{dt}\right)_C = \left(\frac{dT}{dQ}\right)\left(\frac{dQ}{dt}\right) = -\frac{1}{mC}L, \tag{3.18}$$

where the specific heat of the specimen is given by

$$C = \frac{1}{m}\frac{dQ}{dT}. \tag{3.19}$$

When the heater is on, the rate of heating will be

$$\left(\frac{dT}{dt}\right)_H = \left(\frac{dT}{dQ}\right)\left(\frac{dQ_{total}}{dt}\right) = \frac{dT}{dQ}\left(\frac{dQ_{heater}}{dt} - L\right), \tag{3.20}$$

and after eliminating the term $\frac{dT}{dQ}$ one is left with

$$\left(\frac{dT}{dt}\right)_H = \frac{1}{mC}\left(\frac{dQ_{heater}}{dt} - L\right). \tag{3.21}$$

The L term can now be eliminated from the two expressions for the rate of heating:

$$\left(\frac{dT}{dt}\right)_H = \frac{1}{mC}\left(\frac{dQ_{heater}}{dt}\right) + \left(\frac{dT}{dt}\right)_C. \tag{3.22}$$

The first and last term represent the heating and cooling temperature gradients respectively.($\left(\frac{dT}{dt}\right)_C$ will be negative if heat losses predominate). Thus measurements of the heating and cooling temperature gradients, for a given heater power ($\frac{dT}{dQ}$), will enable the heat loss to be eliminated and the specific heat to be determined.

3.3.3 Correction of the temperature rise during heating

If the expression (3.23) for $\left(\frac{dT}{dt}\right)_H$ is integrated over the period of the heating pulse, this will give

$$\Delta T_H = \frac{1}{mC}\Delta Q_{heater} + \Delta T_C \tag{3.23}$$

or

$$C = \frac{1}{m}\frac{\Delta Q_{heater}}{\Delta T_H - \Delta T_C}. \tag{3.24}$$

The quantity ΔT_C represents the amount by which the specimen temperature would have fallen if the heater had not been switched on. By extrapolating the cooling curves measured before and after the heating pulse, ΔT_C can be calculated, or more simply the vertical difference between the two cooling curves represents the total temperature rise,$(\Delta T_H - \Delta T_C)$. The extrapolation process is shown in Figure 3.5.

In practice, we used this technique to check data calculated by computer (especially in the vicinity of transition) because the measurement of $(\Delta T_H - \Delta T_C)$ is easier, and more accurate, than a separete measurement of either ΔT_H or ΔT_C separately. Time lags between the heater switching on and the heat diffusing through the solid will have the effect of 'rounding off' of the points where the heater is switched on and off, as shown in the figure, but this does not affect $(\Delta T_H - \Delta T_C)$. It also becomes apparent that measurements during heating are less important than those of the cooling curves before and after heating.

In an extreme case, the cooling curve would indeed be curved rather than straight. The most pronounced result of this would be that the cooling curves on either side of the heating pulse would have different slopes, and the value of $(\Delta T_H - \Delta T_C)$ would then depend on where the vertical line between the two curves is drawn. Ideally, the line should be drawn at the mid point of the actual heating section. We tried to evaluate only data in which the difference between the slopes is small, so drawing the line at the midpoint of the heating pulse should be reasonably accurate.

3.3.4 Temperature variation of specific heat

The essence of this experiment is to measure how the specific heat varies with temperature, and the measurements should ideally be done with a very small temperature increment $(\Delta T_H - \Delta T_C)$. However, the accuracy of the measurements clearly improves as the temperature increment $(\Delta T_H - \Delta T_C)$ becomes larger. One should be very careful

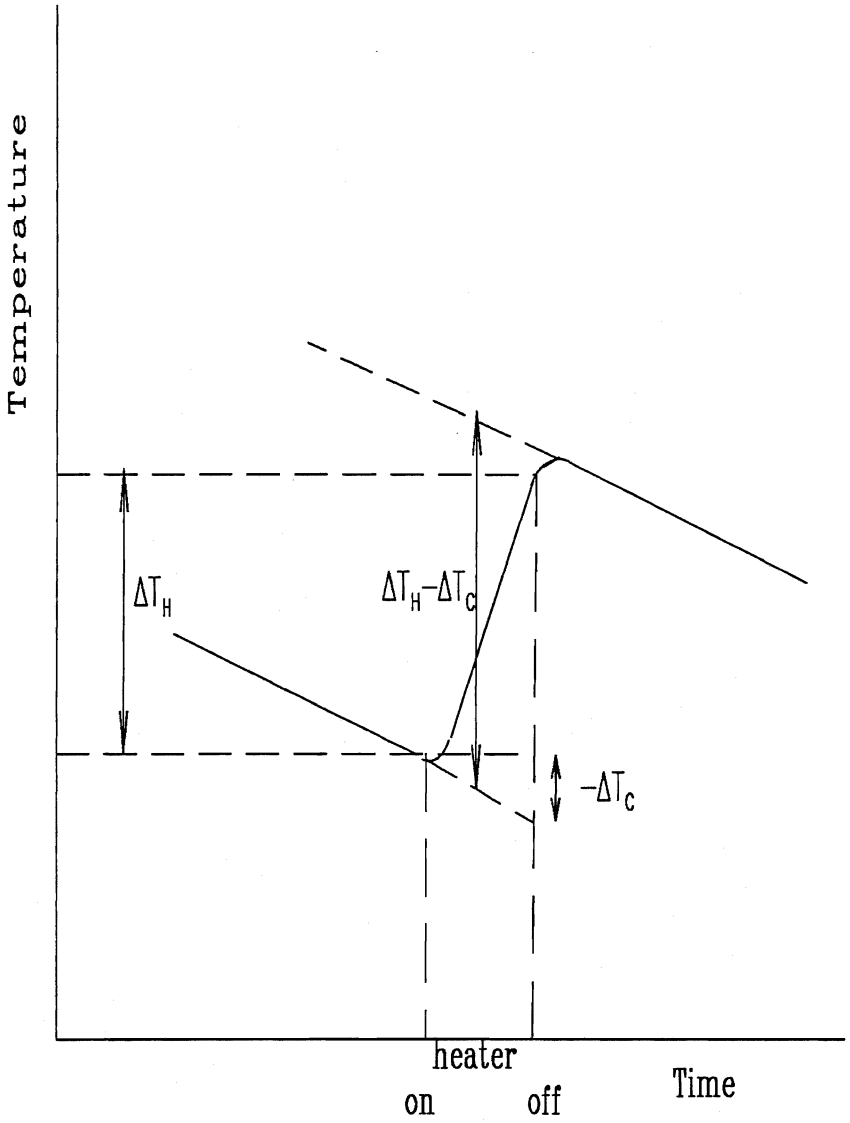

Figure 3.5: **The extrapolation process when temperature is dropping during data collection**

using this technique effect particularly in the measurement of specific heat anomalies because one can simply not see the transition due to its narrowness.

It is shown in the Figure 3.6 that with a temperature increment of 0.1K we have been able to distinguish transitions while with a temperature increment of 0.5K we missed them completely. Thus a compromise is necessary in the temperature increment over which the specific heat is measured.

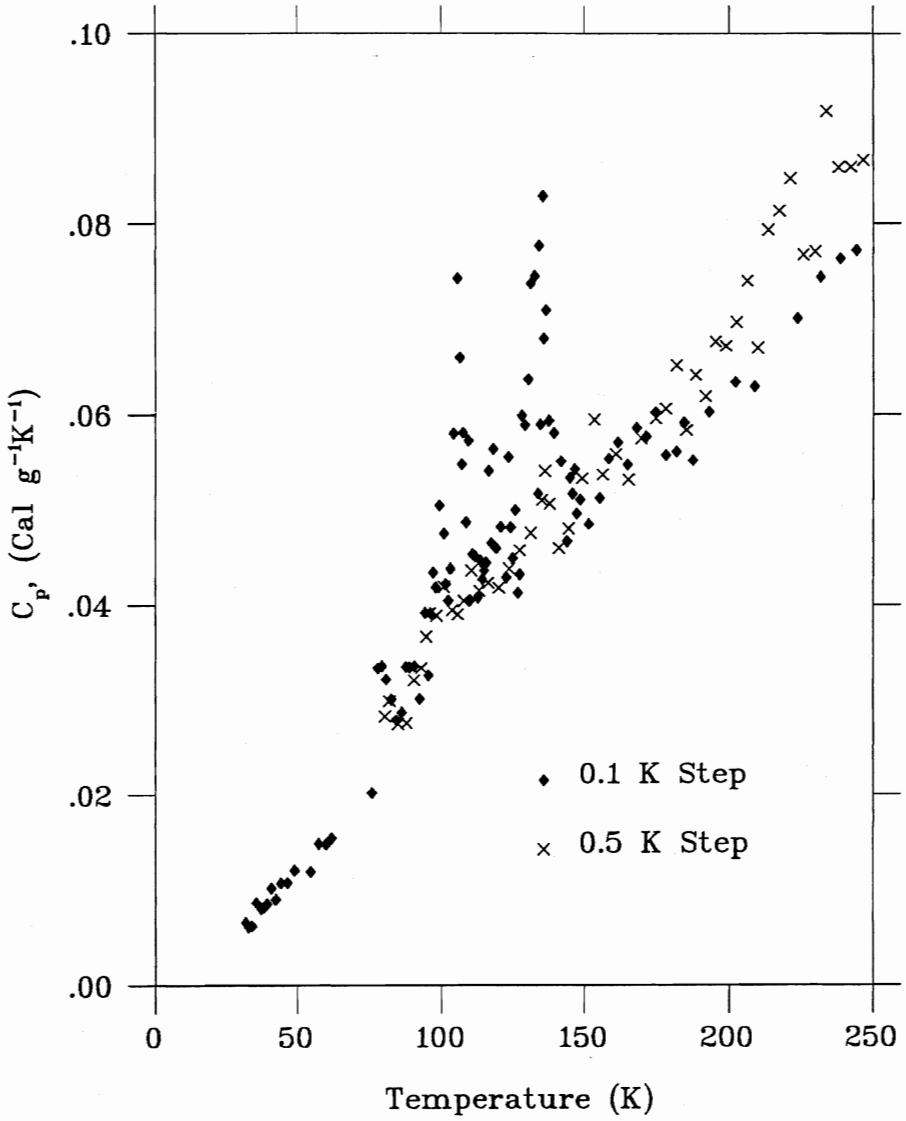

Figure 3.6: **Comparison of data obtained using different temperature increments**
The cross sign is $(\Delta T_H - \Delta T_C) = 0.5K$
The rhombus is $(\Delta T_H - \Delta T_C) = 0.1K$

Chapter 4

Calorimeter Design

Because of the need to minimize heat leaks, the most significant physical property of the cryostat is the thermal conductivity of its components. Alloys, such as stainless steel, have been used as supporting tubes or rods, because of their poor thermal conductivity. On the other hand, copper or brass specimen holders are preferable in the interest of rapid thermal equilibration and good thermal contact between different components.

The central part of the instrument – the platform sample holder – has been described in technical detail in [14]. Figure 4.1 shows the arrangement used. The sample holder consists of a sapphire disc P (diameter 200mm, thickness 2mm) on which a NiCr heater H of about 1KOhm has been evaporated. The sample holder is suspended by three silk threads T inside a copper shield.

A miniature Platinum (or Germanium) thermometer T is glued beside it with varnish and covered with a thin copper foil to improve the thermal contact with the sample. The samples are deposited onto the heater by applying a slight coat of Apiezon – N grease. Two designs have been used to measure the specific heat of the same sample. One of them has a Platinum sample thermometer, and the other – a Germanium sample thermometer. One usually uses a Platinum thermometer to investigate physical properties of the sample in the high temperature range (35K – 300K), whereas the Germanium thermometric resistor is more appropriate at low temperatures (1.5K – 30K). The question of sensitivity of the thermometer is of the important one in the calorimetry. A good thermometer is one which permits sufficient sensitivity in the measuring circuit with the smallest possible

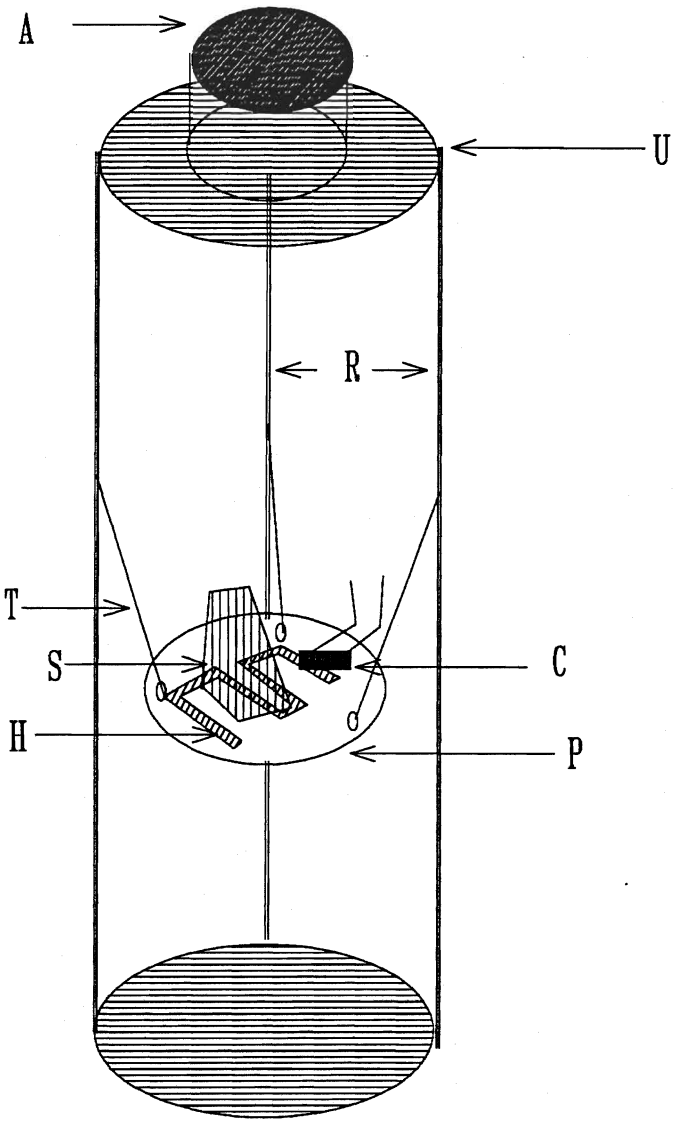

Figure 4.1: **The Sample holder**
A is the thermal anchoring of copper-wire. C is the thermometer to control temperature of sample. H is the sample heater. P is the sapphire block. R is the support for sample holder. U is the upper platform. T is the silk threads. S is the sample.

heat dissipation in the thermometer itself. From this point of view, platinum, germanium, silicon diode thermometers are all satisfactory. Another desirable feature is that the resistance should vary with temperature more or less linearly, since this facilitates the conversion of resistance changes into temperature changes. In this respect, platinum is not very satisfactory below 30° K, and germanium is usually preferred. The special feature of germanium is that it shows nearly linear variation of resistance between 1°K and 20°K (see Figure 4.2). This leads to a good temperature reading. Above 20°K nonlinear temperature variation of the resistance causes errors.

In the literature [15, 16] the Platinum (or Germanium) thermometer is usually housed in an Al_2O_3– block onto which the sample is deposited. In our system, we have removed the sapphire block and used a Ge(or Pt)–resistor as the thermometer which is directly located beside the heater. In this way, the heat capacity of addenda (the background heat capacity) was reduced. The heater area covers a substantial fraction of the sample area, ensuring a good thermal contact and a fast equilibration. Typical extra masses, besides the thermometer and the heater, consist of 4-5 mg of varnish, 25 mg of copper and the electrical wire . All of these form the so-called background. It has been measured in a separate run without the sample.

Thermal conduction down the support tubes and connecting leads is a major source of heat leakage. Because of the high conductivity of copper leads (about 20 times that of stainless steel) they must be as fine as possible. On the other hand, if the copper leads are too fine, Joule heating can become troublesome. The copper leads from higher temperature should always be thermally anchored before reaching the sample, otherwise local heating due to conduction may lead to unreliable measurements.

The electrical wiring to the sample thermometer and heater is made with 0.05 mm diameter copper current leads and phosphor bronze contacts. Their length is about 50

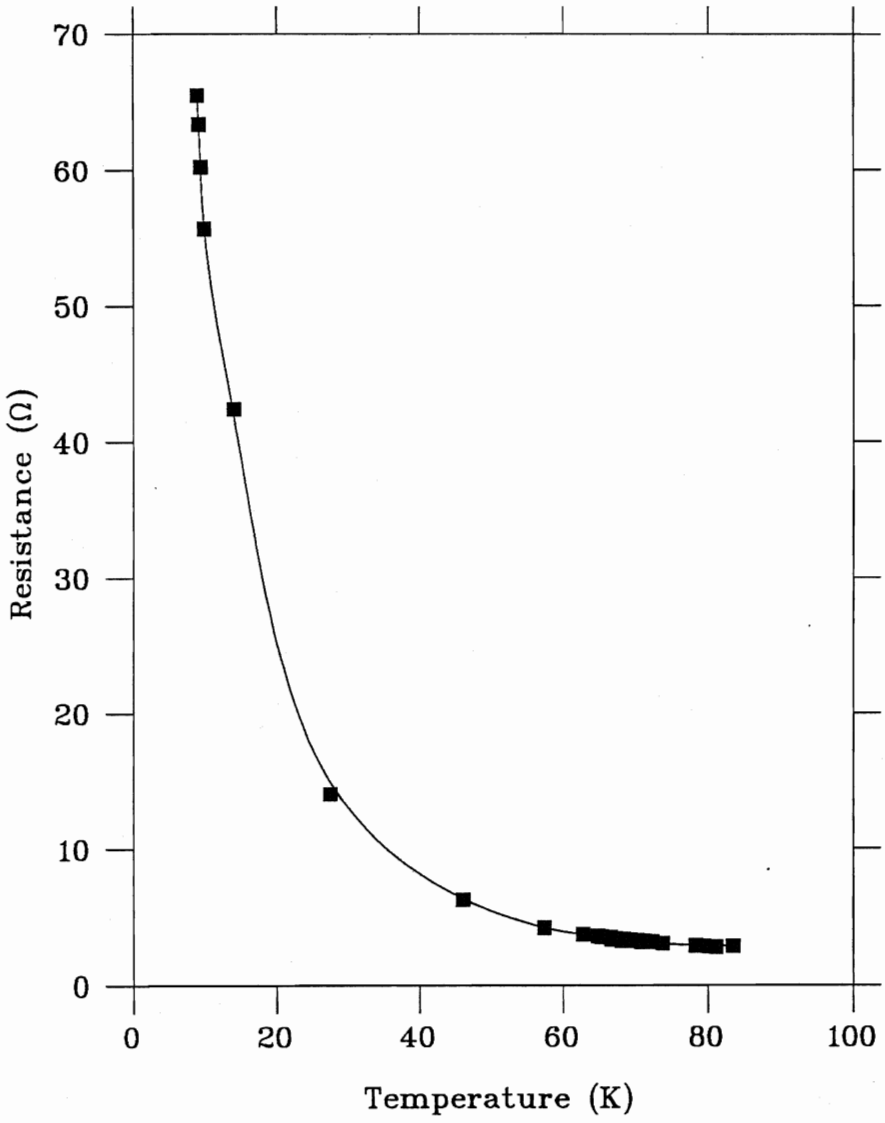

Figure 4.2: **Calibration of the Germanium resistor**

cm. Their resistance is approximately 10 Ω per lead to the heater and 30 Ω per lead to the thermometer. The thermal anchoring consists of a copper block (1cm diameter and 1cm height). The wires are anchored to the copper–block A (Figure 4.1) which is mounted onto the upper platform U of the shield. The copper wires are wound several times around the copper disk (10 mm diameter and 7 mm height) within a groove for better thermal coupling to the corresponding temperature–shield. Varnish is used to improve the thermal contact.

The upper plate U (Figure 4.1) bears the thermal anchoring A, a second thermometer and a heater. The heater is a copper cylinder with a resistance wire heater. Two strands of the heater wire were twisted together and, then, wrapped around the copper cylinder. In this way, the total magnetic field due to the heater is minimized. The temperature of the copper mass is, then, taken to be the so–called bath temperature. The heater power is controlled by a LakeShore DRC-91C Temperature Controller such that the bath temperature remains constant at a specified set point of temperature. At temperatures below 28K, the accuracy of the LakeShore Temperature Controller is 0.03K. Above 28K, the system accuracy gradually moderates to a typical value of $\pm 75m$K. The standard set point temperature can be set to 0.1 degree. In our experiment we were not able to reach temperatures lower than 1.6K.

The copper cylinder with the heater may be unscrewed to give access to the experimental space. This heated copper mass is held from the vacuum can by two thin-walled copper tubes with Teflon rods at their ends. These rods provided rigid support to the sample mount as well as thermal isolation from the copper bath.

Figure 4.3 shows a general view of the cryostat. The vacuum can (50 mm in diameter and 160 mm in length) is connected to the the pump by a thin–walled stainless steel tube V (Figure 4.3). The vacuum can is sealed by indium wire.

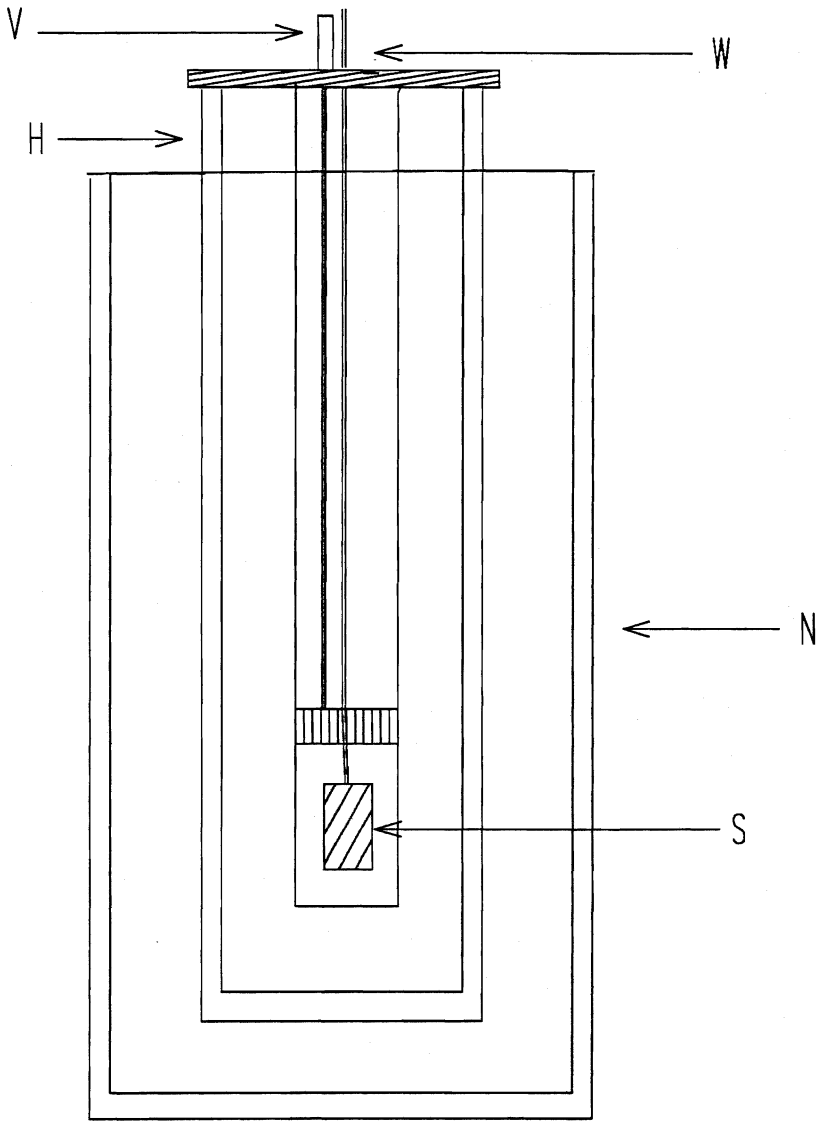

Figure 4.3: **The Cryostat. General view**
V is the vacuum tube. W is the electrical connectors. H is the inner dewar (usually for liquid Helium). N is the outer dewar (usually for liquid Nitrogen). S is the sample chamber.

The cryostat, then, has been surrounded by a system of dewars containing liquid helium *H* (Figure 4.3) and liquid nitrogen *N*. The outer dewar containing liquid nitrogen is essential in order to limit the heat leak into the cryostat by radiation.

In the precooling stage of an experiment, it is common practice to introduce a little helium gas as an exchange gas in order to speed up the cooling process. However, the helium gas tends to be strongly adsorbed onto the sample surface and thus one must then pump the system for a long time (usually for 2–3 hours) before starting the measurement.

Experiments at temperatures below 4.2K can be carried out easily in cryostats using liquid helium . Liquid helium boils under atmospheric pressure at 4.2K. By reducing the vapor pressure a temperature between 4.2 K and about 1K can be reached by pumping on liquid helium.

This experimental system fulfills the requirements of a good sample holder for adiabatic calorimetry :

1. Easy handling and quick exchange of the samples by putting the crystal onto sapphire disc.

2. Very good thermal contact.

3. High reproducibility .

4. Low heat capacity of the addenda.

The experimental system has been tested with a high-purity sample of Copper using the Step Heating method . Figures 4.4 and 4.5 show the actual experimental points and reference data of the specific heat of Copper. The agreement between them indicates the reliability of our experimental system.

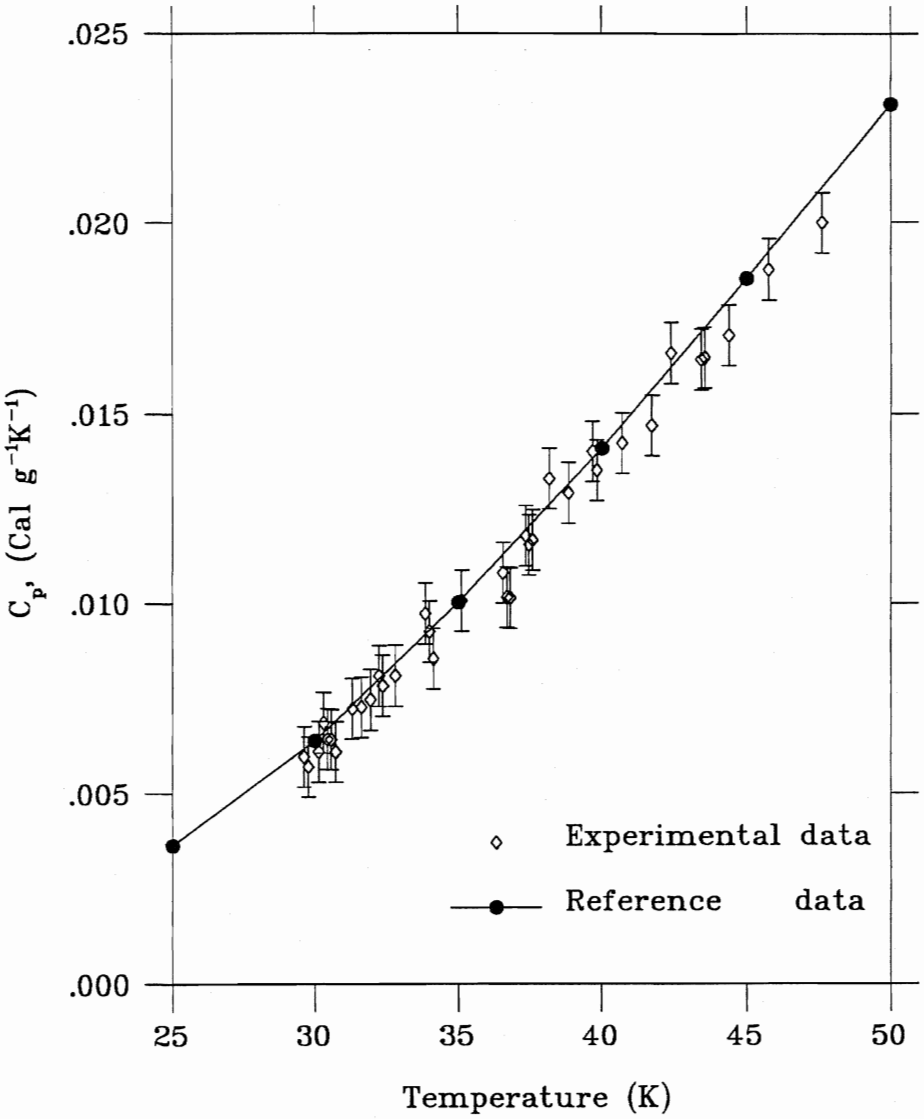

Figure 4.4: **The specific heat of Copper (temperature range 30–50K)**

There are two significant problems of LTC (low temperature calorimetry) due to dramatic changes in the physical properties of solid below 100K:

- a tremendous reduction of thermal energy (i.e. C_p) by a factor of $10^3 - -10^6$ occurs on cooling any material from 150 K to liquid helium temperature;

- this strong variation of $C_p(T)$ is accompanied by a similar intensive change of the thermal interactions between the sample and its surrounding (shield). This interaction, however, is different in its temperature dependence from that of C_p. Whereas below 10K the heat transfer from sample to shield is governed by the thermal conduction proportional to the temperature difference ΔT along the electrical connections, the radiational heat exchange is the dominant part above 40K; that heat exchange is proportional to $T^3\Delta T$.

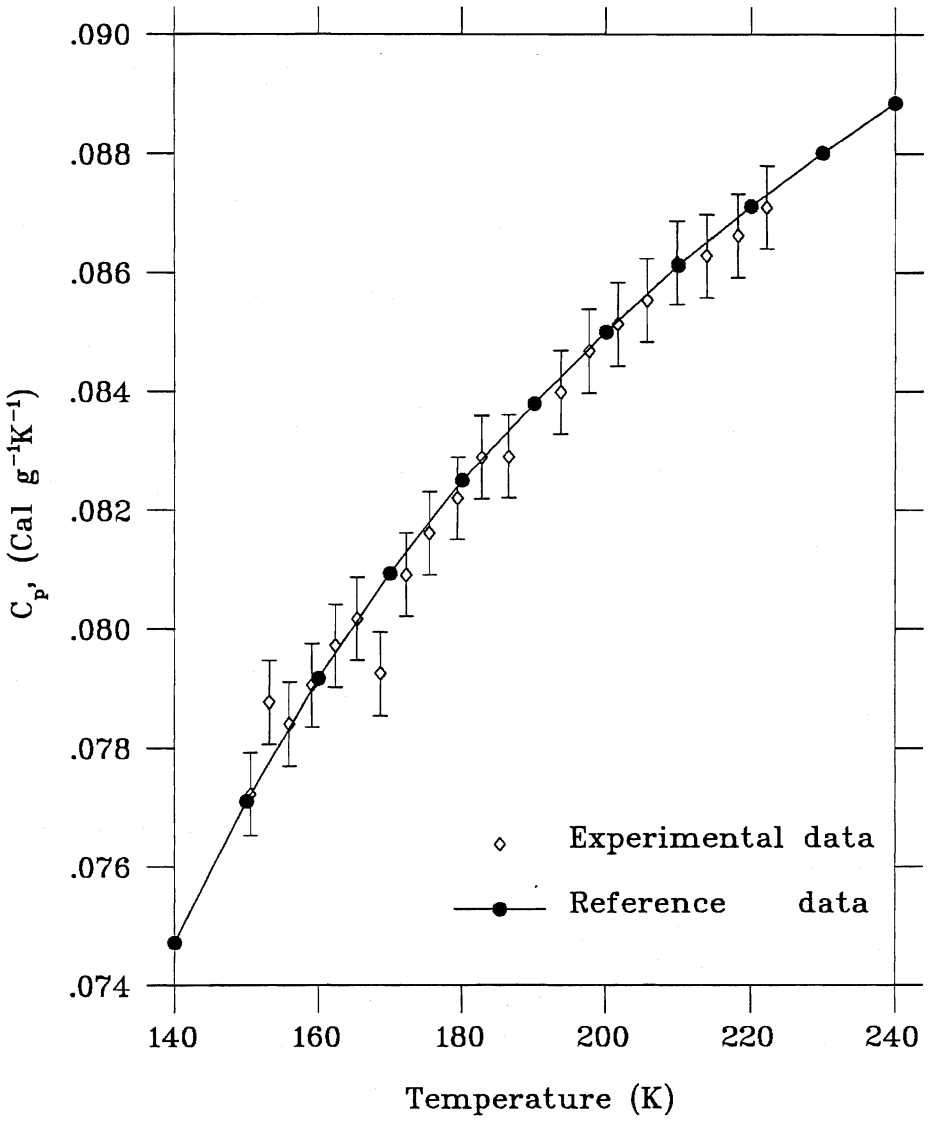

Figure 4.5: **The specific heat of Copper (temperature range 140–220K)**

Chapter 5

Specific Heat of UPd_2Si_2

5.1 UPd_2Si_2

The low temperature normal state of UPd_2Si_2 has been the subject of several neutron–scattering [2], magnetic susceptibility [2, 4] and Hall-effect [4] studies. UPd_2Si_2 in the form of polycrystalline sample, was first reported [9] to undergo antiferromagnetic ordering below 97K (magnetic susceptibility measurement), with spin density wave peaks at 40K (powder neutron diffraction).

Others [2, 4, 3] presented the results of elastic neutron scattering, magnetic susceptibility, electrical resistivity and Hall effect on single crystal samples of UPd_2Si_2.

The single crystal, which we have used in the specific heat experiments reported herein, was grown at McMaster [12] by a modified triple-arc Czochraski method. UPd_2Si_2 belongs [2] to the $ThCr_2Si_2$ crystal structure type with space group I4/mmm. The arrangement of the atoms in a unit cell is as shown in Figure 5.1. The uranium atoms occupy the 2a position to form a simple body-centered tetragonal sublattice. The palladium atoms are in the 4d position and the silicon atoms are in the 4e positions. The Bragg reflections of the nuclear unit cell are of the form $h + k + l = 2n$. The lattice constants a and c as shown in Figure 5.1 are $a = 4.077 \pm 0.002\mathring{A}$ and $c = 10.046 \pm 0.001\mathring{A}$ at 12 K.

The magnetic neutron scattering measurement [2] indicates that the magnetic moments are localized on Uranium atoms. In zero magnetic field there is a simple body-

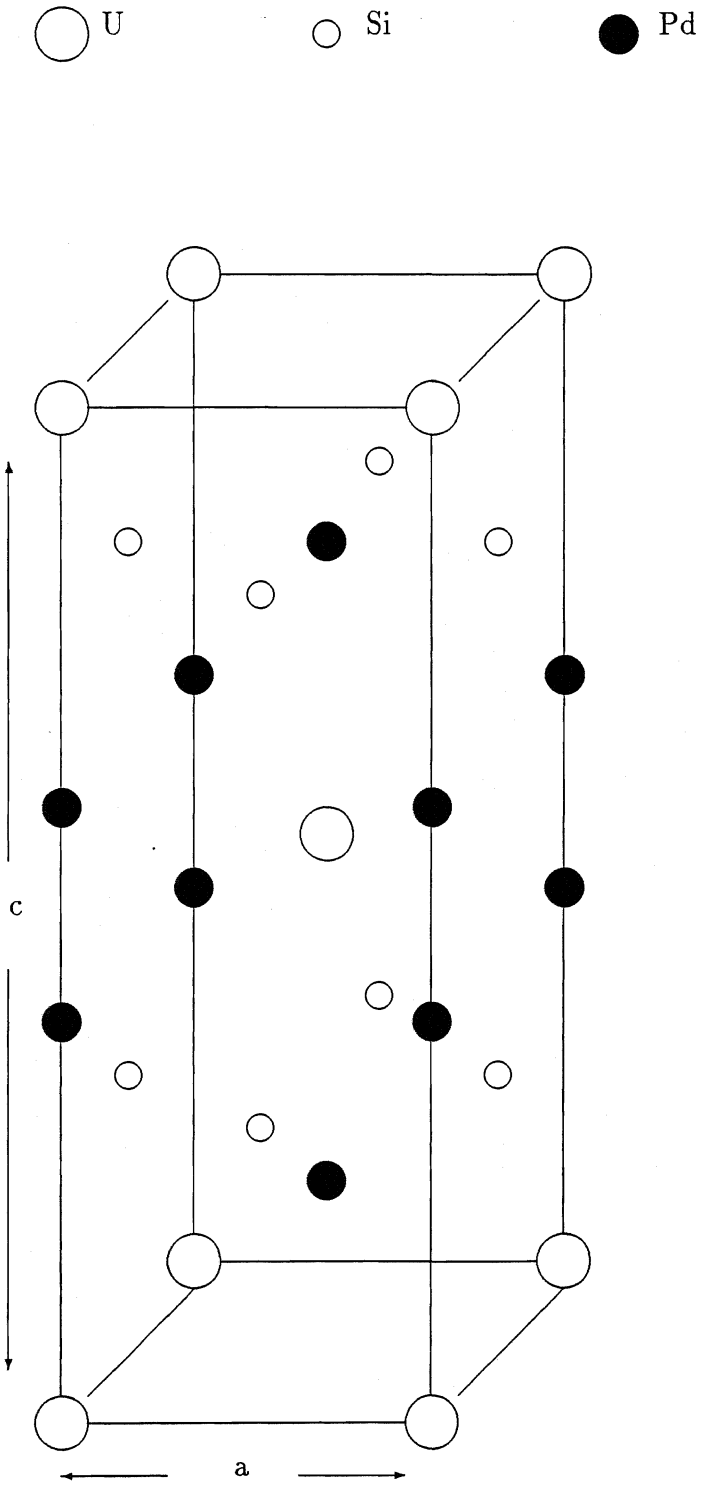

Figure 5.1: **The body-centered tetragonal crystal structure of** UPd_2Si_2

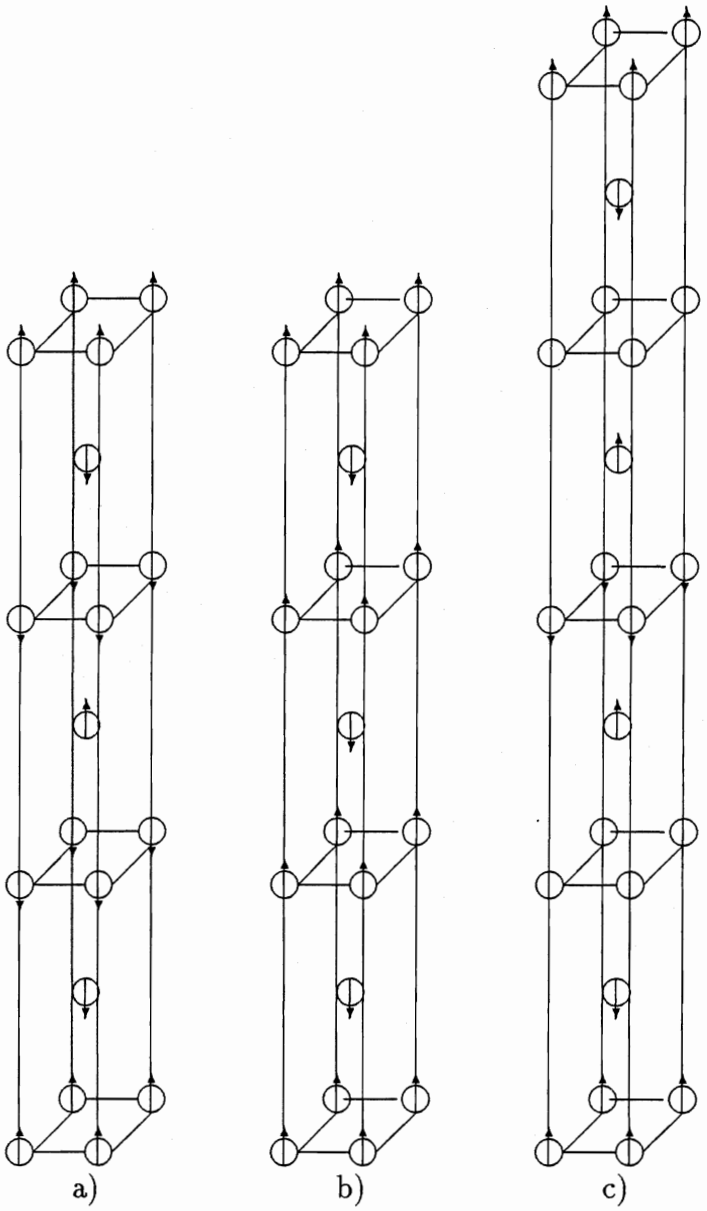

Figure 5.2: **Magnetic structure of U-sublattice in the three phases**
a) commensurate spin-density-wave structure (does not exist in this compound, but is shown here for completeness),
b) antiferromagnetic structure of UPd_2Si_2 for the temperature range < 108K,
c) incommensurate spin-density-wave phase of UPd_2Si_2 for the temperature range 108–136K.

centered antiferromagnetic structure for the temperature up to 108K. Between 108K and the Neel temperature which is around 136K there is an incommensurate longitudinal spin-density-wave phase (see Figure 5.2). These results show no indication of a phase transition at 40K.

The resistivity measurement done by M. Barati [4] exhibits a $\ln(T)$ dependence at high temperature (above 150K) whereas T^2 behavior is observed at low temperature (below 30K). A T^2 fit to the low temperature data gave a coefficient of about $4.62 \times 10^3 \mu\Omega cm$. This number is much larger than that of a usual metal but not big enough compared to typical heavy fermion compounds such as UPt_3 or URu_2Si_2 [6]. There are no linear or T^3 terms, so that the large resistivity is not due to electron-phonon scattering.

The elastic neutron-scattering and magnetization measurements have been described in [2, 4]. The magnetization curves show the transition at 108K which can be referred to as the transition between the antiferromagnetic and spin–density wave states because of a considerable decrease of the magnetic susceptibility. A clear magnetic transition with hysteresis was observed below 136K. The behavior of the magnetic susceptibility is Curie-Weiss like above 150K which starts to increase as the temperature decreases.

To complete the picture of work done on UPd_2Si_2, the Hall effect set of measurements[4] should be mentioned here. At temperatures between 4.2 and 100K, there was the ordinary Hall effect of conduction electrons. Above 100K, the scattering of the conduction electrons by the localized moments caused a large Hall coefficient and a sharp maximum at 130K [4]. It was reported that the electron-phonon scattering process is negligible and the so-called skew-scattering term which is related to skew–scattering of the conduction electrons by the localized moment plays a big role during scattering. It is interesting to notice that all of the parameters of UPd_2Si_2 are very similar to those of heavy fermion compounds.

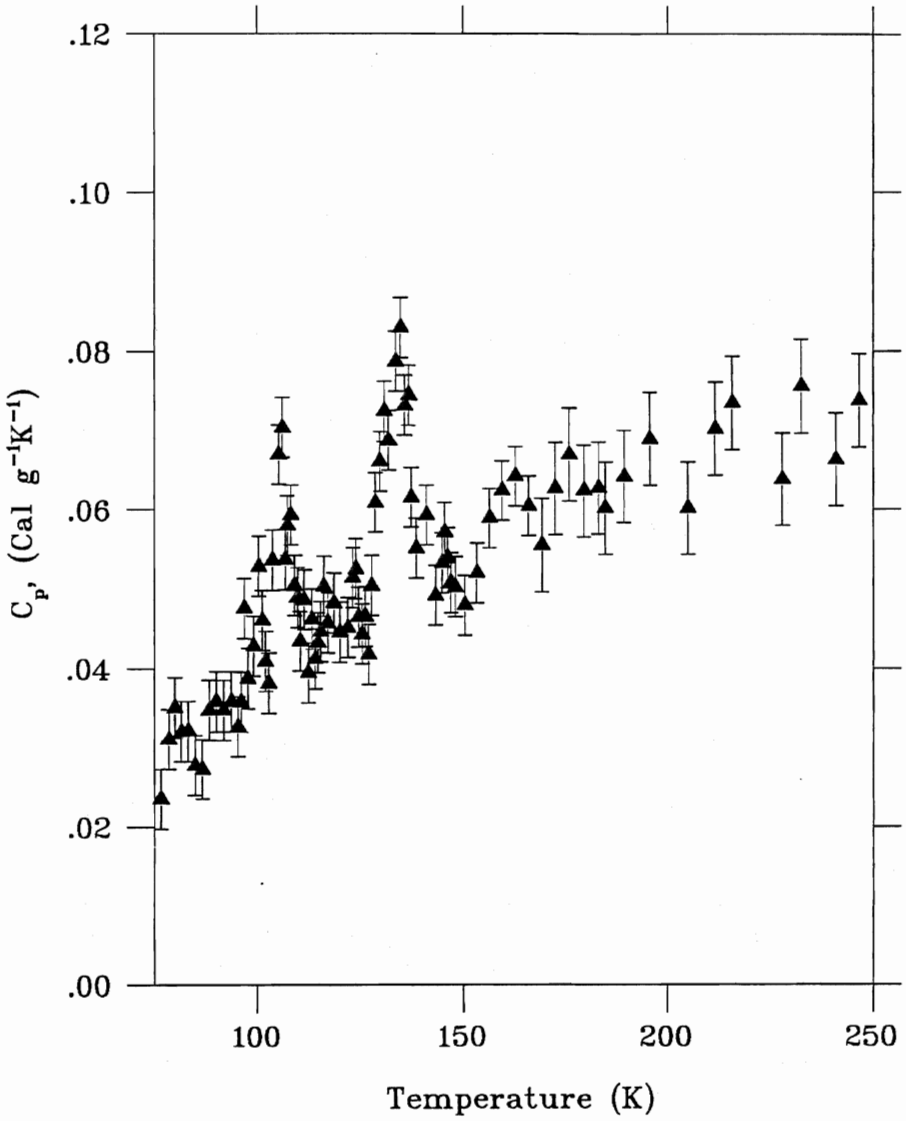

Figure 5.3: **Specific heat of the UPd_2Si_2 single crystal as a function of temperature(temperature range $75K - 250K$)**

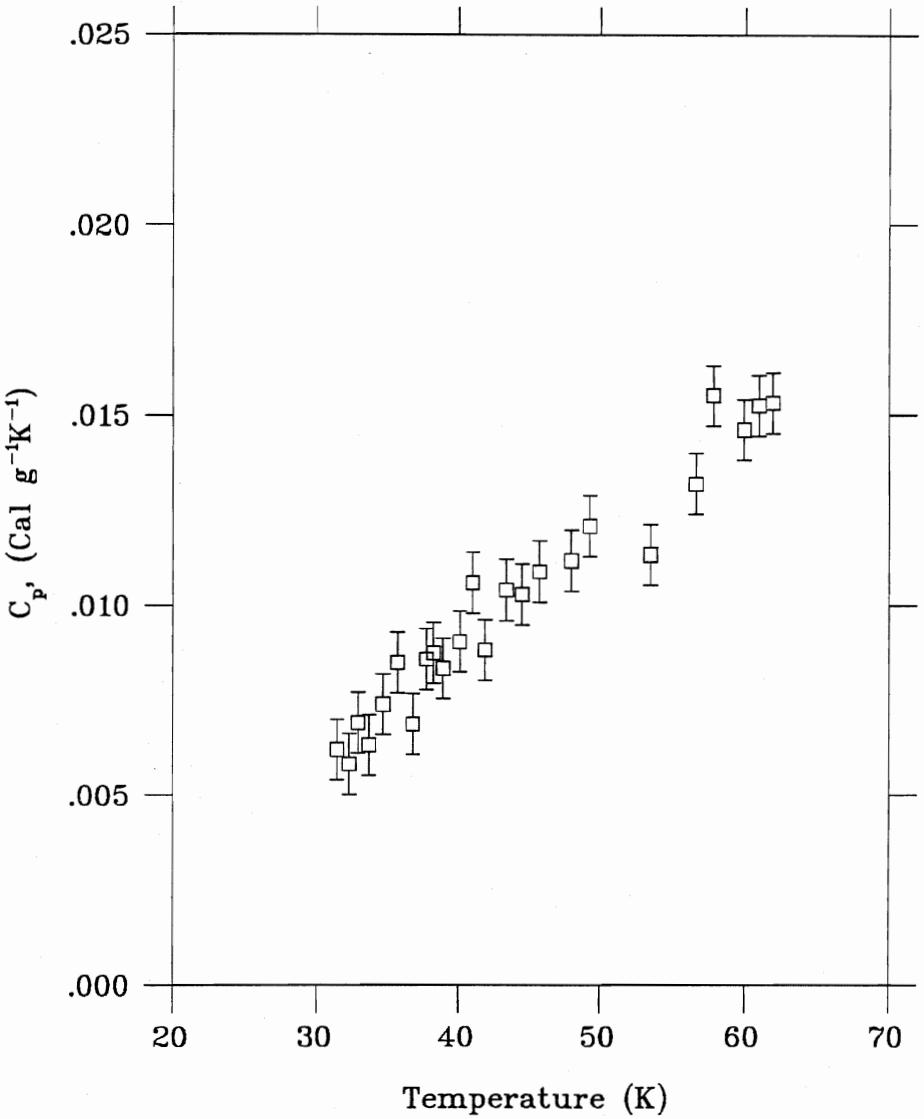

Figure 5.4: **Specific heat of the UPd_2Si_2 single crystal as a function of temperature(temperature range $30K - 70K$)**

5.2 Experiment

5.2.1 Specific heat data at high temperature (Step method)

The process of collecting data was discussed in Chapter 3. For each temperature, the corresponding C_P value has been obtained by averaging three experimentally determined specific heat data points. The heat capacity from 75K to 250K is presented in Figure 5.3. The two distinct maxima at 108K and 136K indicate two magnetic phase transitions. On the low-temperature side of the transitions the specific heat rises first gradually and then rapidly. When it has reached its maximum value, it drops very rapidly to a much lower value . The general form of these curves is explained [11] by assuming that once the transition to configurations of the higher energy begins, then all atoms are participating in the transition, and it takes longer to change their configuration to the new phase. When the transition is very close to culmination, there are just a small number of atoms which still need to change their configuration. This is the reason for the rapid rise which is observed after the relatively slow increase at the beginning of the transition.

One large peak in Figure 5.3 is evident at 136K indicating the onset of the paramagnetic phase.

Both peaks are in excellent agreement with previous susceptibility and neutron-diffraction results [2, 4], in which the magnetic phase transitions at 108 and 136K have been observed.

Neutron-elastic-scattering results [2] indicate that this compound has two magnetically ordered phases. At a temperature lower than 108K, a simple body-centered tetragonal antiferromagnet exists with an order moment of $(2.3 \pm 0.3)\mu_B$. This state is followed by a different antiferromagnetically ordered state with an incommensurate spin density wave and with the same magnitude of magnetic moment. This state belongs to the

temperature range from 108K to 136K. There is a critical phase transition to the paramagnetic phase at 136K. The low-temperature heat capacity are presented in Figure 5.4. There is no indication of a phase transition between 30K and 70K. This supports the recent study of UPd_2Si_2 by elastic neutron scattering [2, 4]. This may be compared with the results for a polycrystal of UPd_2Si_2 in which a phase transition was observed at 40K by neutron scattering experiments [9].

5.2.2 Specific heat data using Sweep method

All data described above have been taken using the Step method. Another method of measuring heat capacity – the Sweep method – will be discussed here. The results of these measurements are shown in Figures 5.5and 5.6, respectively.

Two series of measurements were made on the UPd_2Si_2 sample. The first was made in the region of the first transition, i.e. for temperature from 80 to 115K, and the second in the vicinity of second transition, i.e. from 120 to 190K.

As it has been described in Section 3.1.1, a constant power of 7mW was supplied to the sample. The heat is provided by the sample heater. The bath heater supplied pulses to the surrounding sample, so that the shield temperature is that of the sample. The bath temperature was constantly compared with the sample temperature (so–called feedback mechanism). The resulting temperature versus time diagrams for the heating curves are shown in Figure 5.6 and in Figure 5.5 (upper graphs).

The mathematical description of the specific heat using the Sweep method is given by the formula (see Figure 3.3)

$$C(T) = \frac{I_H U_H}{\frac{dT}{dt}}. \tag{5.1}$$

Thus, the specific heat is proportional to the reciprocal of the temperature–time derivative. After having performed a complete experiment, the derivatives of the data

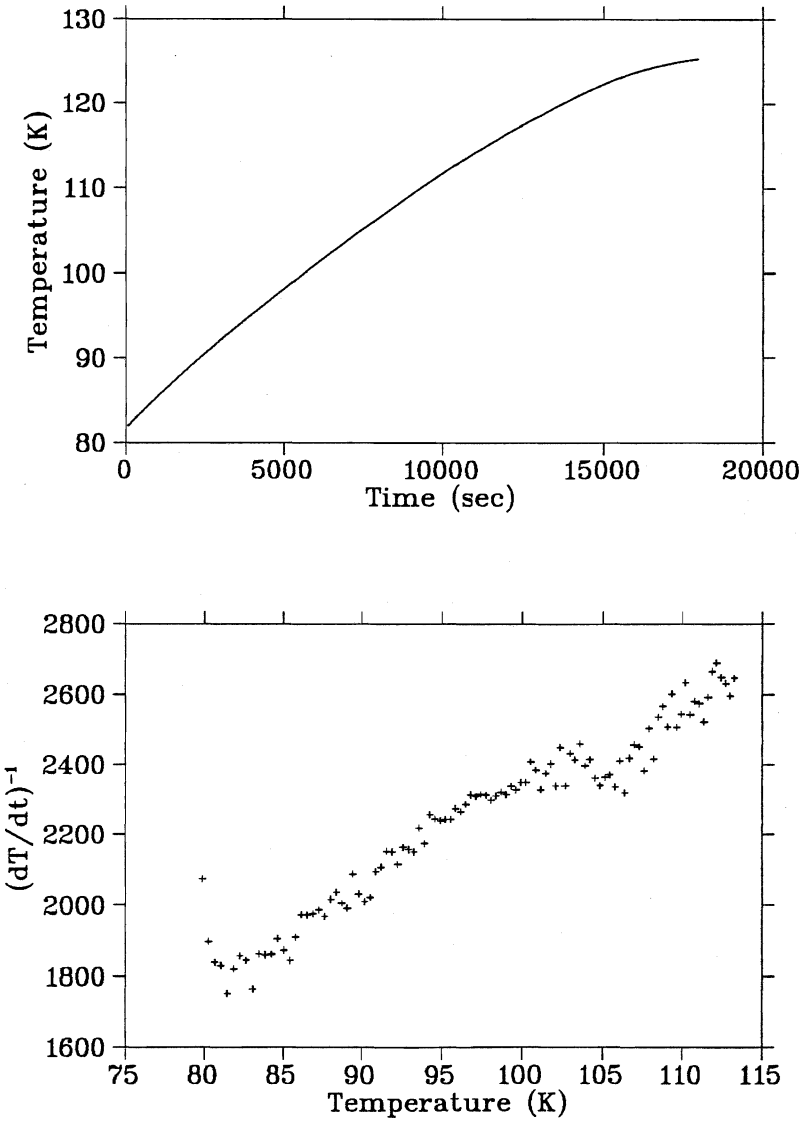

Figure 5.5: **Specific heat of UPd_2Si_2 from measurements using the Sweep method**
The raw data directly from experiment is shown in the top graph . The bottom graph shows the reciprocal of the derivative of temperature with respect to time obtained from raw data points versus temperature.

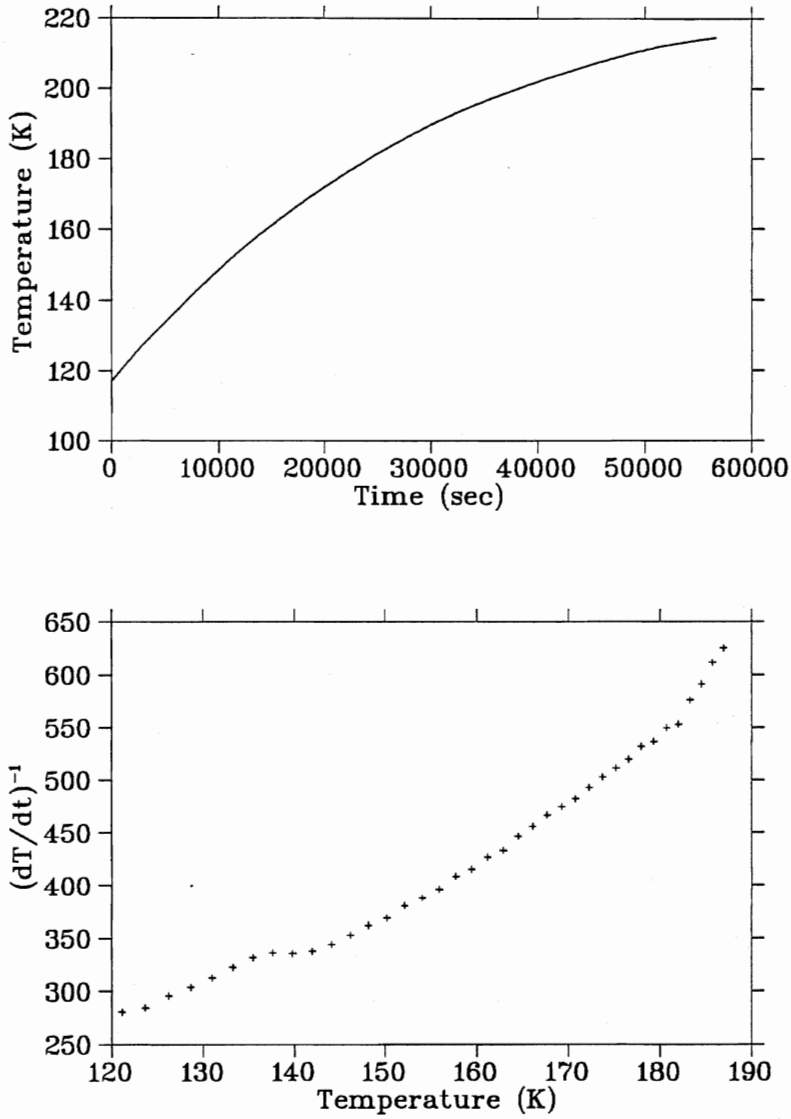

Figure 5.6: **Specific heat of UPd_2Si_2 from measurements using Sweep method**
The raw data directly from experiment is shown in the top graph. The bottom graph gives the reciprocal of the derivative of temperature with respect to time obtained from raw data points versus temperature.

were taken. Due to the sensitivity of the method to mechanical vibrations and thermal fluctuation, the computed derivative varies significantly. To avoid this, the specific heat data have been separated from experimental noise and fluctuation using a program based on an RC–filter method (see Appendix) in order to get a smooth curve. The lower graphs found in Figures 5.5 and 5.6 are the results obtained from such a calculation.

Two phase transitions are clearly noticeable in lower graphs of Figures 5.5 and 5.6. The transition from an antiferromagnetic state to the spin density wave phase is shifted to a lower temperature compared to the measurement done by the Step method. It occurred at 104K (see Figure 5.5) and not at 108K (see Figure 5.3). Whereas the transition from the spin density wave phase to the paramagnetic state remained the same at 136K (see Figure 5.6 and Figure 5.3). The shift of the transition temperature can be caused by a temperature difference between the sample and the bath (the feedback mechanism is not ideal). The jumps in specific heat data at the transition temperatures obtained by the Sweep method are not as pronounced as those that appeared in data measured by the Step heating method. This can be explained by several reasons:

- It is essential that thermal equilibrium within the sample and between the sample thermometer be rapid. There were several gradients of temperature between sample-thermometer-varnish-heater in the experimental system.

- The Sweep method is very sensitive to vibration. Vibrations cause fluctuations in the temperature-time dependence diagram which generate problems in the calculating of the derivative.

- The averaging of a number of points during calculation of the derivative leads to a suppression of the transition peaks.

5.2.3 Specific heat data at low temperature

For a better analysis of the low-temperature specific heat of UPd_2Si_2, the data are plotted as $\frac{C}{T}$ vs T^2 in Figure 5.7. One can clearly see an upturn around 4K. This sharp rise of $\frac{C}{T}$ has been observed in previous experiments on heavy fermion materials. There are several explanations for this anomaly.

The first heavy fermion system $CeCu_2Si_2$ [7] is explained to be caused by a the "Kondo-lattice" anomaly. In a dilute Kondo system, one expects a compensation of the local impurity moments by the conduction electrons to remove the spin-degeneracy entropy associated with each local spin. This according to several authors [20, 10] is the reason for the increase of the specific heat at very low temperatures. In the study of UPt_3 by Stewart et.al. [5], the observed upturn in the specific heat has been attributed to the spin-fluctuation term $T^3\ln(T)$, and the temperature dependence of C_P was fitted by the formula $\beta T^3 + \gamma T + \delta T^3 \ln T$. Attempts to fit the C_P data for UPd_2Si_2 to the form $\beta T^3 + \gamma T + \delta T^3 \ln T$ failed completely, whereas this form fits the UPt_3 data [5] quite well. One can find the actual fit in Figure 5.8. A peak in C_P for $CeAl_3$ was identified by Mahoney et. al. [21] as a Schottky anomaly. Investigating the high-T_C superconductor $La_{2-x}Sr_xCuO_4$, several groups [22, 23] referred to a similar 'upturn' as a Schottky anomaly due to magnetic impurities. A concentration of magnetic impurities as small as 0.07% per Cu gives rise to a Schottky peak. It is interesting that $La_{2-x}Sr_xCuO_4$ is similar to UPd_2Si_2 in that it has an antiferromagnetic phase as well as an incommensurate magnetic fluctuation phase.

Figure 5.7 shows the data points and a fit which includes a Schottky anomaly term. At temperatures well above the peak , $C_{Schottky} \sim T^{-2}$ and the total specific heat will be of the form $C = \gamma T + \beta T^3 + \delta T^{-2}$. As we can see, this fit is in very good agreement with the experimental data. The analysis of the low-temperature data for UPd_2Si_2 into

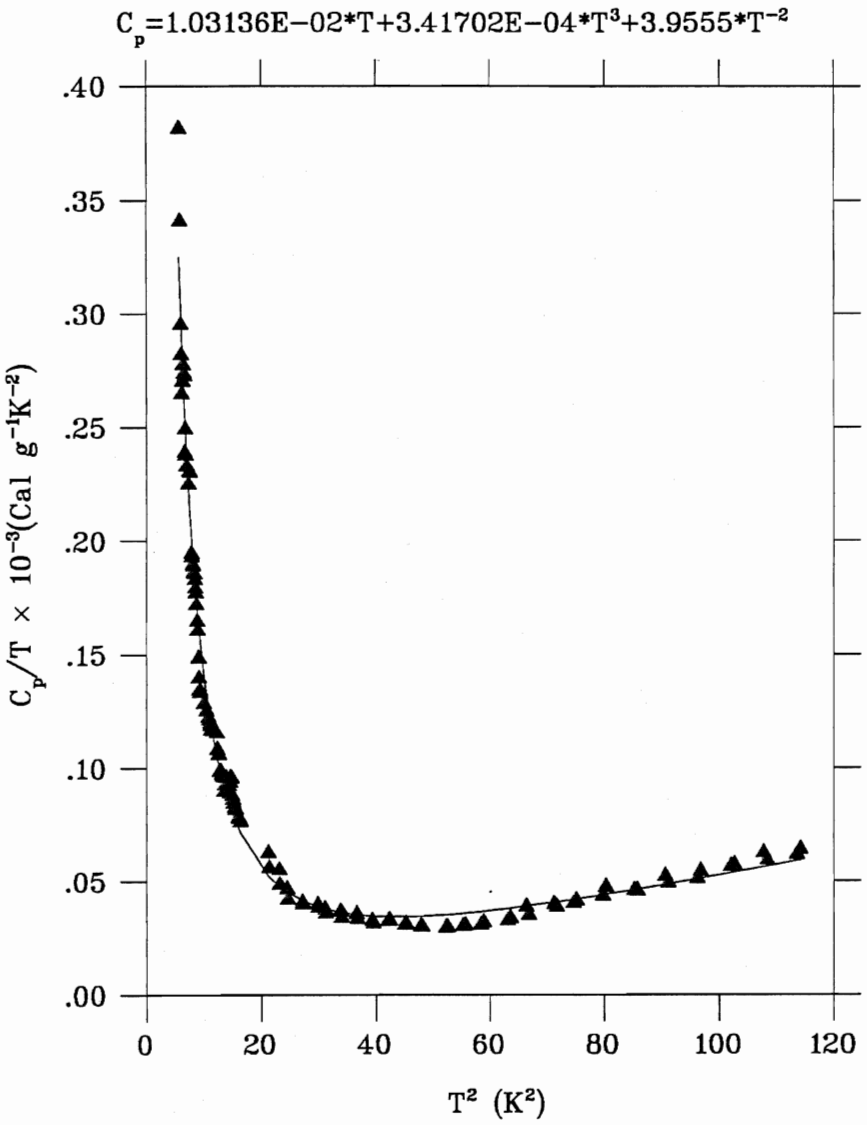

Figure 5.7: **Specific heat of the UPd_2Si_2 single crystal as a function of temperature(temperature range 2K – 10K)**
The solid line drawn is a fit to $C = \gamma T + \beta T^3 + \delta T^{-2}$.

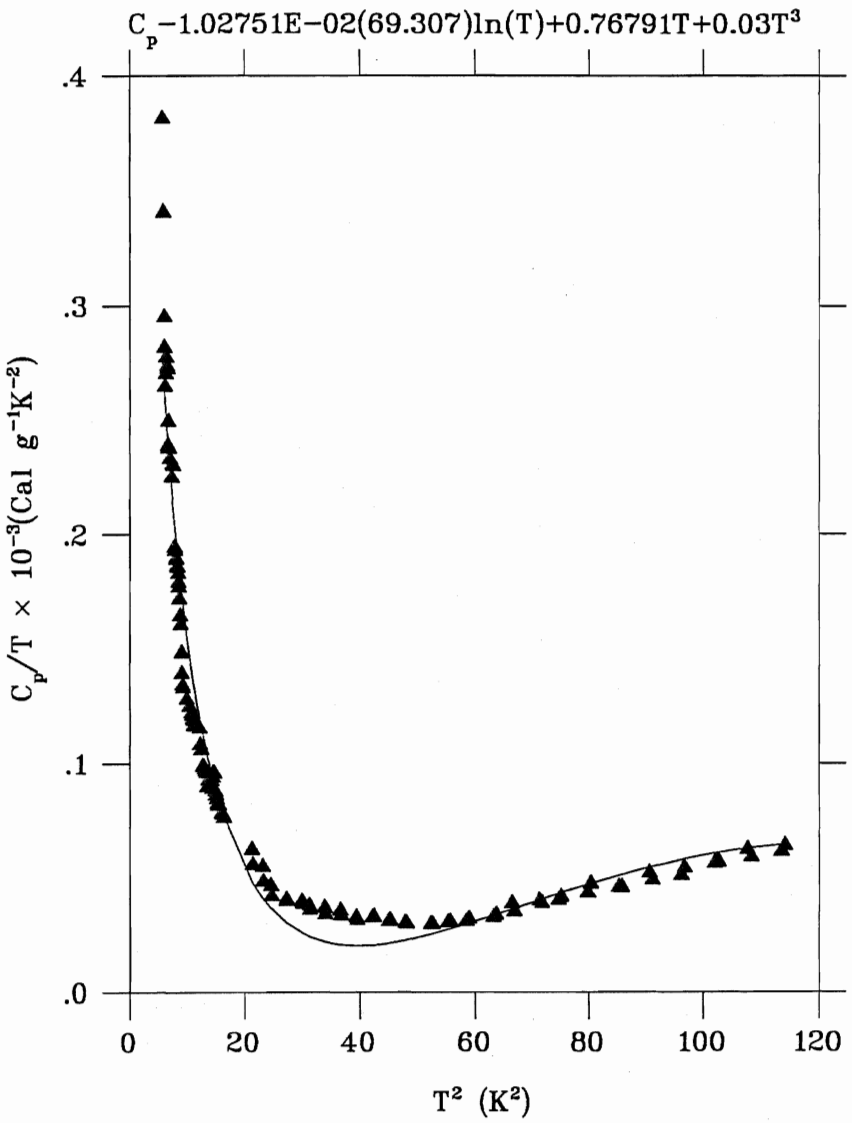

Figure 5.8: **Specific heat of the UPd_2Si_2**
The solid line through the data a fit to $C = \gamma T + \beta T^3 + \delta T^3 \ln T$.

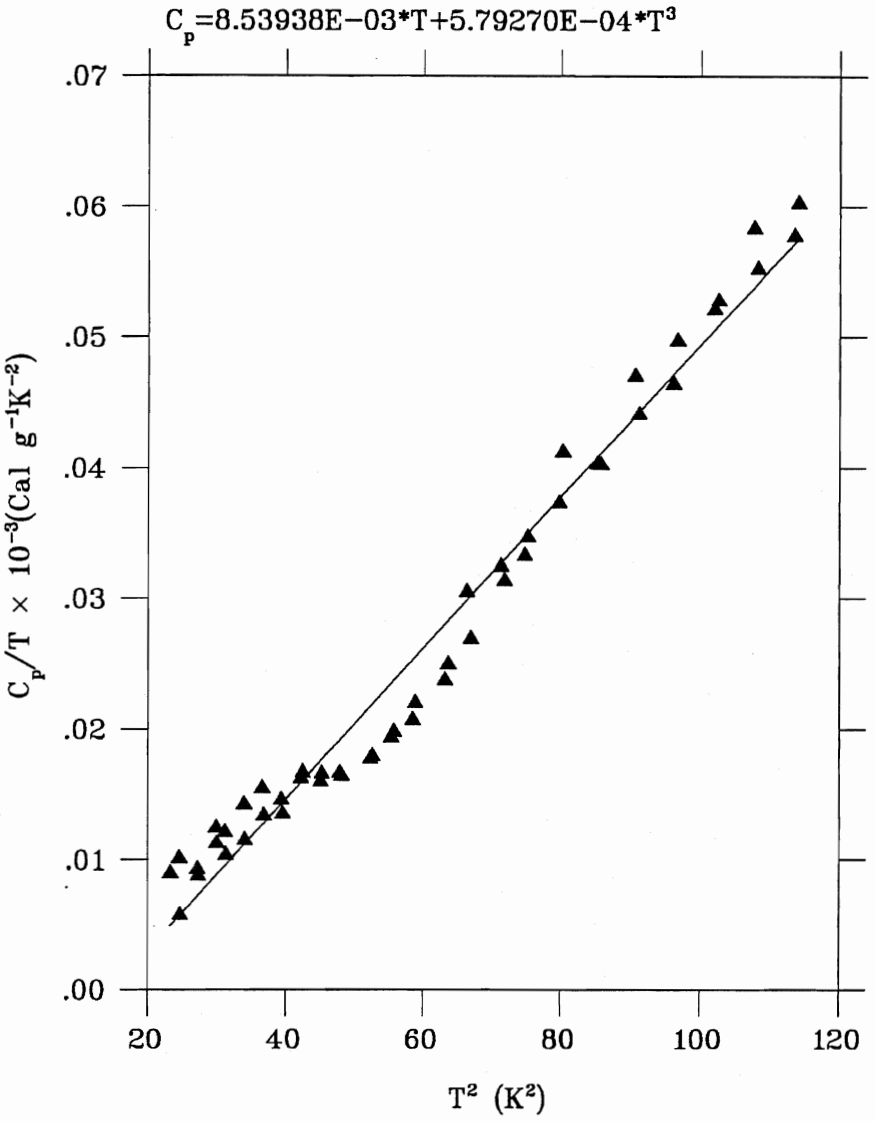

Figure 5.9: **Specific heat of UPd_2Si_2**
The "Schottky-like" anomaly is subtracted away.
The solid line through the data is a fit to $\frac{C}{T} = \gamma + \beta T^2$.

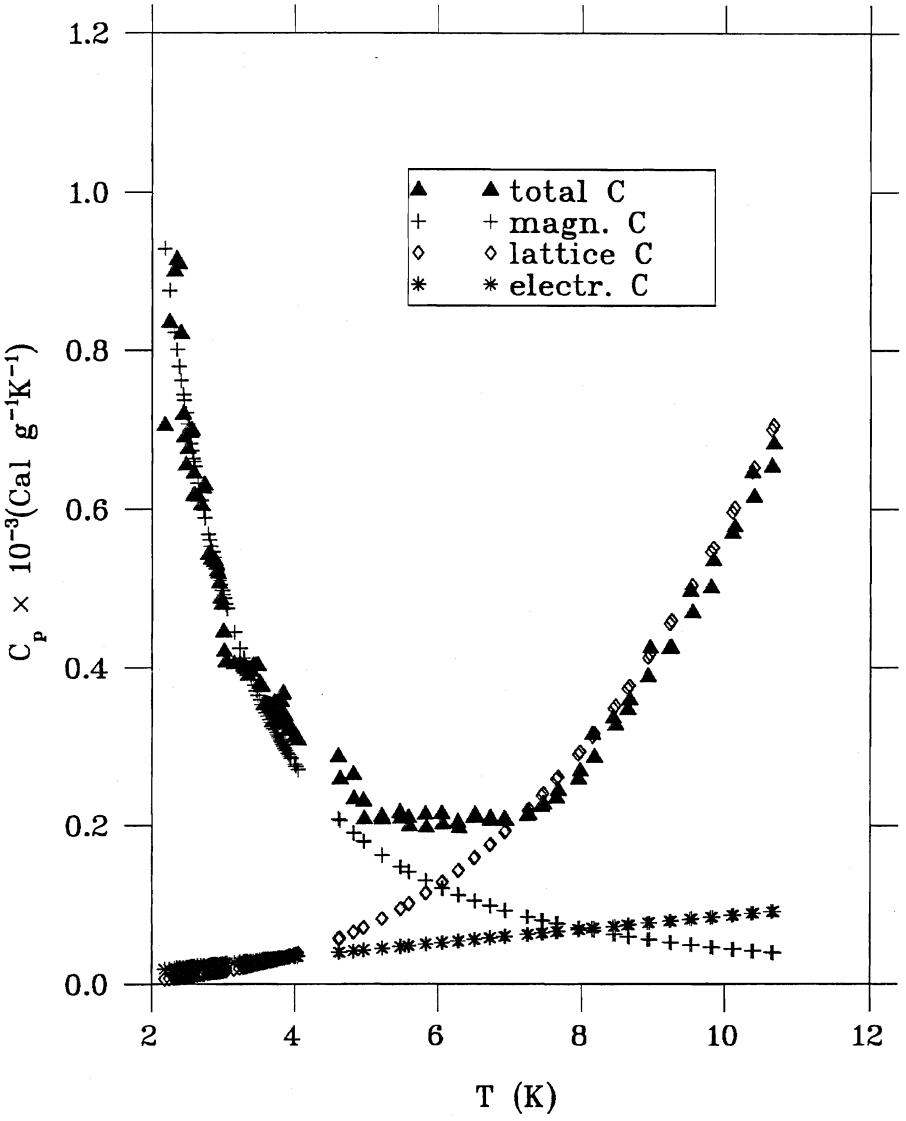

Figure 5.10: **Three contributions to the low-temperature specific heat of UPd_2Si_2**
△ is the experimental data of the total specific heat. + is the Schottky anomaly contribution due to magnetic impurities. ◇ is the lattice contribution. ∗ is the electronic contribution.

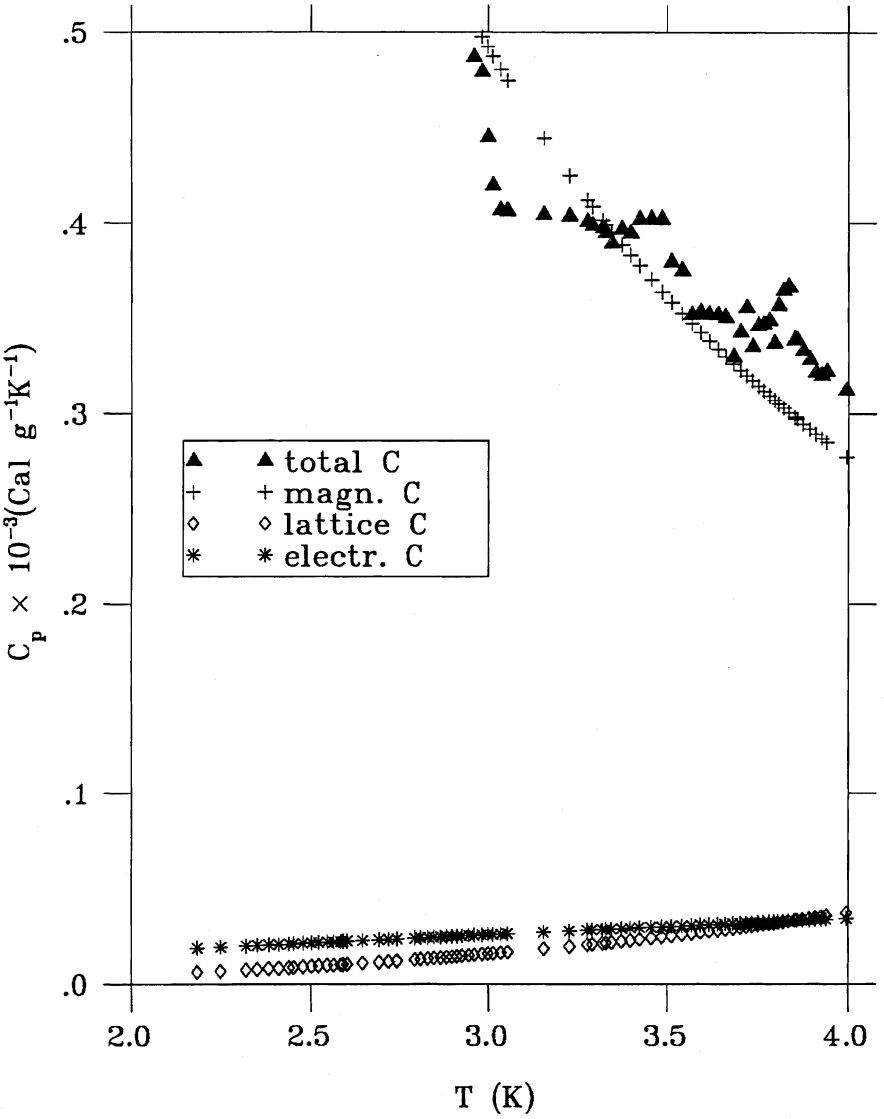

Figure 5.11: **Temperature dependence of the different contributions to the specific heat of UPd_2Si_2**
△ is the experimental data of the total specific heat. + is the Schottky anomaly contribution due to magnetic impurities. ◇is the lattice contribution. $*$ is the electronic contribution.

components, electronic, lattice and Schottky-like, is illustrated in Figure 5.10. The temperature dependence of the low-temperature specific heat can be summarized as follows. The contribution of the lattice vibration begins to exceed that of the electrons as the temperature is raised above 4K, and above 8K practically only the lattice contribution plays a big role. The points at temperatures > 8K in the Figure 5.10 which belong to the specific heat due to lattice vibrations are perfectly lined up with the total specific heat at these temperatures. The low-temperature region of Figure 5.10 is produced in magnified form in Figure 5.11 for a better demonstration of the fact that the electronic contribution predominates over lattice contribution below 4K, but that the 'Schottky-like' contribution is the most prevalent.

Figure Number	β, $\frac{Cal}{gK}$	β, $\frac{mJ}{gK}$	Θ_D, K	γ, $\frac{Cal}{gK^2}$	γ, $\frac{mJ}{gK^2}$
Fig.5.7	3.41702×10^{-7}	0.72416	138.972	1.03136×10^{-6}	21.85
Fig.5.8	0.03×10^{-3}	63.579	31.268	0.76791	1627435
Fig.5.9	5.7927×10^{-7}	1.2276	116.55	8.53938×10^{-6}	18.097

Table 5.1: Parameters β, γ and Debye temperature calculated using different fits

The next step in the data analysis was to eliminate from all low temperature data the 'Schottky-like' contribution assuming that the coefficient of the T^{-2} term is temperature independent. After the 'Schottky - like ' anomaly has been subtracted, a graph of $\frac{C}{T}$ against T^2 should be a straight line with a slope of β and an intercept on the $\frac{C}{T}$ axis of γ. In this way, both Θ_D and γ may be calculated from the data. We must , of course, make certain that the measurements are made in the true T^3 region, for the lattice contribution to the specific heat, i.e. at temperatures below $\frac{\Theta_D}{10}$. The plot of $\frac{C}{T}$ against T^2 is shown in Figure 5.9 and it will be noted that a good straight line is obtained . All fits have been done using the graphing software PLOTDATA (χ^2= 0.31082E-03 for

Fig.5.9; $\chi^2 = 0.10669E-01$ for Fig.5.8; $\chi^2 = 0.1022E-02$ for Fig.5.7).

The electronic specific heat parameter γ and calculated Debye temperatures using eq.3.6 from all low temperature graphs mentioned above are given in Table 5.1. As one can notice, the value of γ obtained from the $C_P = \gamma T + \beta T^3 + \delta T^3 \ln T$ fit does not make any sense, i.e. the 'upturn' in the specific heat cannot be related to the spin–fluctuation term $\delta T^3 \ln T$. The electronic specific heat parameters γ, calculated from Figure 5.7 and Figure 5.9, are very close to each other. From our point of view the second one is more precise, because the dominant Schottky anomaly contribution has been eliminated.

The value of the electronic specific heat coefficient γ estimated from the polynomial fit to the data is compared with various heavy fermion compounds and copper as a representative normal metal in Table 5.2 (The values for URu_2Si_2 and UPt_3 were taken from [6]; UNi_2Si_2 - from [3]; Cu - from [8]). One can notice that γ of UPd_2Si_2 is larger than that of the usual metals but not high enough for conventional heavy fermion compounds such as URu_2Si_2, and UPt_3.

The large increase in γ for these materials, compared to the values in metals (e.g. Cu), is not understood at this time.

	γ, $\frac{mJ}{gK^2}$
UPd_2Si_2	18.97
UNi_2Si_2	22
URu_2Si_2	180
UPt_3	450
Cu	0.7

Table 5.2: Electronic specific heat coefficient γ for various compounds

Chapter 6

Conclusions

A low temperature calorimeter has been built. The specific heat of UPd_2Si_2 has been measured in the temperature range from 2 to 250K.

Two transition peaks have been observed. The peak at 108K is associated with the first order transition from an antiferromagnetic phase to an incommensurate spin density wave. The peak at 136K is associated with a transition to the high temperature paramagnetic phase. Both peaks are in good agreement with the previous elastic neutron scattering results of Shemirani *et.al.* and with the electrical resistivity measurements by M. Barati *et.al.*. We find no indication of the phase transition at 40K reported in [9]. There is a drastic increase in the specific heat below about 4K. We have attributed this increase to a Schottky anomaly rather than to spin-fluctuations, based on fits to the low temperature data. The electronic contribution to the specific heat was found to be linear in temperature with a coefficient $\gamma = 19\frac{mJ}{gK^2}$. This value is much higher than what is found in a typical metal, but is much lower than what has been measured in prototype heavy-fermion materials.

Appendix A

Listing of RC-filtering program

```
program smoothmain
implicit double precision(a-h,o-z)
c parameter(npoints=3398) ! dec1.rec
c parameter(npoints=10439)! nove.rec
parameter(npoints=7826/2) ! dec2.rec
c parameter(npoints=1000)
dimension x(npoints),y1(npoints),y2(npoints),y3(npoints)
dimension y4(npoints),y5(npoints)
#include <gl/fgl.h>
#include <gl/fdevice.h>

c call testrc(npoints)
call initgraph

call rdata(x,y1,npoints)
c call cdata(x,y1,npoints)
c call draw(x,y1,npoints)

call derivative(x,y1,npoints,y2)
call color(BLACK)
do i=1,npoints
  y2(i)=1./y2(i)
enddo
c call draw(y1,y2,npoints)

call rc(x,y1,npoints,y2)
call rc(x,y2,npoints,y3)
call derivative(x,y3,npoints,y4)
c call smooth(y4,npoints,y5)
call color(RED)
do i=1,npoints
  y5(i)=1./y4(i)
enddo
call draw(y1,y5,npoints)
```

```
open(1,file='output')
do i=1,npoints
  write(1,*)y1(i),y5(i)
enddo
close(1)
call closegraph
stop
end



subroutine rc(x,y,n,yo)
implicit double precision(a-h,o-z)
c parameter (tau1=0.00005,tau2=tau1,tau=tau1*tau2/(tau1+tau2),
c     +          nmax=100000)
parameter (nmax=100000)
dimension x(n),y(n),aux(nmax),yo(n)
print *,'Enter tau1=tau2'
read *,tau1
tau2=tau1
tau=tau1*tau2/(tau1+tau2)
yo(1)=tau/tau1*y(1)
do i=1,n-1
  b=(y(i+1)-y(i))/(x(i+1)-x(i))
  e=exp((x(i)-x(i+1))/tau)
  yo(i+1)=(yo(i)-tau/tau1*(y(i)-b*tau))*e+tau/tau1*(y(i+1)-b*tau)
enddo
do i=1,n
  yo(i)=yo(i)*(tau1+tau2)/tau2
enddo
return
end


subroutine smooth(x,n,y)
implicit double precision(a-h,o-z)
parameter (ns=10)
dimension x(n),y(n)
do i=1,ns
  y(i)=x(i)
enddo
do i=1+ns,n-ns
  a=0.
```

```
  do j=i-ns,i+ns
    a=a+x(j)
  enddo
  a=a/(2.*ns+1)
  y(i)=a
enddo
do i=n-ns+1,n
  y(i)=x(i)
enddo
return
end


subroutine integrate(x,y,n,yi)
implicit double precision(a-h,o-z)
dimension x(n),y(n),yi(n)
yi(1)=0.
do i=2,n
  yi(i)=yi(i-1)+y(i)*(x(i)-x(i-1))
enddo
return
end



subroutine derivative(x,y,n,yd)
implicit double precision(a-h,o-z)
dimension x(n),y(n),yd(n)
yd(1)=(y(2)-y(1))/(x(2)-x(1))
do i=2,n-1
  yd(i)=((y(i)-y(i-1))/(x(i)-x(i-1))+(y(i+1)-y(i))/(x(i+1)-x(i)))/2.
enddo
yd(n)=(y(n-1)-y(n))/(x(n-1)-x(n))
return
end


double precision function rfnc(x)
implicit double precision(a-h,o-z)
parameter(a=0.5,b=200.,bmin=0.2,bmax=0.25)
add=0
if (x.ge.bmin .and. x.le.bmax) add=b*(x-bmin)*(bmax-x)
rfnc=a*x*(2-x)+add
```

```
return
end


subroutine cdata(x,y,n)
implicit double precision(a-h,o-z)
dimension x(n),y(n)
do i=1,n
  a=(i-1.)/(n-1.)
  x(i)=a
  y(i)=rfnc(a)
enddo
return
end


subroutine rdata(x,y,n)
implicit double precision(a-h,o-z)
dimension x(n),y(n)
c open(1,file='dec1.rec')
c open(1,file='nove.rec')
open(1,file='dec2.rec')
read(1,10) x(1),y(1)
do i=2,n
  read(1,10) x(i),y(i)
 10   format(f10.4,x,f8.4)
enddo
close(1)
return
end


subroutine mdata(x,y,n)
implicit double precision(a-h,o-z)
parameter (am=0.01,num=200,iseed=92347)
dimension x(n),y(n)
call srand(iseed)
pi=4*atan(1.)
do i=1,n
  x(i)=x(i)+am*sin((i-1.)/(n-1.)*2*pi*num)
c   x(i)=x(i)+am*rand()
enddo
return
```

```
end


subroutine draw(x,y,n)
implicit double precision(a-h,o-z)
dimension x(n),y(n)
xmin=x(n/2)
xmax=x(n/2)
ymin=y(n/2)
ymax=y(n/2)
do i=100,n
          if (x(i).gt.xmax) xmax=x(i)
          if (x(i).lt.xmin) xmin=x(i)
          if (y(i).gt.ymax) ymax=y(i)
          if (y(i).lt.ymin) ymin=y(i)
enddo
 1 continue
c ymin=1700
c ymax=2900
print *,''
print *,'x',xmin,xmax
print *,'y',ymin,ymax
xg=(x(1)-xmin)/(xmax-xmin)
yg=(y(1)-ymin)/(ymax-ymin)
call pen(xg,yg)
do i=1,n
  xg=(x(i)-xmin)/(xmax-xmin)
  yg=(y(i)-ymin)/(ymax-ymin)
  call line(xg,yg)
enddo
return
print *,''
print *,'New ymin,ymax? (1/0)'
read *,i
if (i.eq.1) then
  print *,'Enter ymin'
  read *,ymin
  print *,'Enter ymax'
  read *,ymax
  go to 1
endif
return
end
```

```
        subroutine initgraph
#include <gl/fgl.h>
#include <gl/fdevice.h>
        integer*4 id
        call foregr
        call prefpo(610,1010,400,800)
        id=winope('Test Window',11)
        call color(BLUE)
        call clear
        call color(WHITE)
 1      if (getbut(7)) goto 1
        return
        end



        subroutine line(x,y)
        double precision x,y
        logical getbut
        aux1=400.*x
        aux2=400.*y
        call draw2(aux1,aux2)
 1      if (getbut(7)) goto 1
        return
        end

        subroutine pen(x,y)
        double precision x,y
        logical getbut
        aux1=400.*x
        aux2=400.*y
        call move2(aux1,aux2)
 1      if (getbut(7)) goto 1
        return
        end
```

```
        subroutine closegraph
        logical getbut
        print *,''
        print *,'Hit Esc to continue...'
10      if (.not.getbut(7)) goto 10
        call gexit
        return
        end


subroutine step(x,y,n)
implicit double precision(a-h,o-z)
dimension x(n),y(n)
do i=1,n/6
  y(i)=(i-1.)/(n/6-1)*0.5
  x(i)=(i-1.)/(n-1.)
enddo
do i=n/6+1,n/3
  y(i)=0.5
  x(i)=(i-1.)/(n-1.)
enddo
do i=n/3+1,2*n/3
  y(i)=0.6
  x(i)=(i-1.)/(n-1.)
enddo
do i=2*n/3+1,n
  y(i)=0.4
  x(i)=(i-1.)/(n-1.)
enddo
return
end


subroutine testrc(n)
implicit double precision(a-h,o-z)
parameter (nmax=100000)
dimension x(nmax),y(nmax),y1(nmax)
#include <gl/fgl.h>
#include <gl/fdevice.h>
call initgraph
```

```
call step(x,y,n)
call draw(x,y,n)
call rc(x,y,n,y1)
call color(RED)
call draw(x,y1,n)
call closegraph
return
end
```

Bibliography

[1] T.T.M.Palstra *et. al.*, Phys.Rev.Lett.,**55**,1985,2727.

[2] B.Shemirani, H.Lin, M.F. Collins, C.V. Stager and J.D. Garrett, W.J.L. Bueyers and Z.Tun, Phys. Rev B,**48**,22,1993,16500-16504.

[3] Y.B.Ning, J.D.Garrett, and W.R.Datars, Phys. Rev B, **42**,13,1990,8780-8782.

[4] M.Barati,W.R. Datars, T.R. Chien,C.V.Stager, and J.D.Garrett, Rev B, **48**,23,1993,16926-16928.

[5] G.R. Stewart, Z. Fisk,J.O. Willis, and J.L. Smith, Phys. Rev. Lett., **52**, 1984,679.

[6] Z.Fisk, H.R. Ott,T.M.Rice, and J.L.Smith, Nature **320**,1986,124

[7] F.Steglich, J.Aarts, C.D.Bredl, W.Lieke, D.Meschede, W.Fratz, and H.Schafer, Phys.Rev.Lett. **43**,1979,1892.

[8] E.S.P. Gopal, Specific heats at low temperatures, 1966.

[9] H. Ptasiewicz-Bak, J.Leciejewicz, and A.Zygmunt, J.Phys.,**11**,1981,1224.

[10] D.Gignoux,D.Schmitt, M.Zerguine, C.Ayache and E.Bonjour, Physica Lett. A,**117**,3,1986,145-149.

[11] E.Gmelin, Thermochimica Acta,**29**, 1979,1-39 .

[12] A.A.L. Dawson, W.R. Datars, J.D. Garrett, and F.S. Razavi, J. Phys. **11**,1985,1225.

[13] A.Junod,J.Phys.E, Sci. Inst., **12**,1979,945-52.

[14] E.Gmelin and K.Ripka, Cryogenic **21**,1981,117-118.

[15] E.Gmelin and K.Ripka, Thermochimica Acta, European Symposium on Thermal Analysis and Calorimetry – 84.

[16] E.Gmelin, Thermochimica Acta,**110**, 1987, 183-208.

[17] C.Domb, Magnetism, edited by G.K.Rado and H.Suhl, Academic, N.Y.,1965,VIIA,p.1

[18] S. Doniach,and S.Engelberg, Phys. Rev. Lett.,**17**,1966, 750.

[19] W.F. Brinkman, and S.Engelberg, Phys. Rev.,**169**, 1968, 4117.

[20] W. Assmus, M. Herrmann,U.Rauchschwable, S.Riegel, W.Lieke, H.Spille, S. Horn , G. Weber, F.Steglich, and G. Cordier, Phys. Rev. Lett.,**52**,1984,469.

[21] J.V. Mahoney, V.U.S.Rao, W.E.Wallace, R.S. Craig, and N.G. Nereson, Phys Rev.B **9**,1974,154.

[22] T.E.Mason, G.Aeppli, S.M.Hayden, A.P.Ramirez, and H.A.Mook, phys Rev. Lett.,**71**,6,1993,919-922.

[23] R.A.Fisher, N.E.Phillips, and J.E.Gordon, The specific heat of Thallium Oxide Superconductors, a chapter in Thallium-Based High Temperature Superconductors, A.M.Hermann and J.V.Yakhmi, Eds.,Marcel Dekker, New York, NY,1992.

[24] H.M.Staudenmaier, Physics experiments using PCs, Springer-Verlag, New York, 1992.